scientific reports

OPEN

Head kinematic variability is minimal near preferred cadence and independent of the vestibular control of locomotion

Liam H. Foulger[1], Calvin Kuo[2,3], Romeo Chua[1] & Jean-Sébastien Blouin[1,4,5]✉

The unstable nature of our bipedal posture requires continuous feedback to maintain internal estimates of self-motion and generate appropriate balance-correcting responses. This feedback control process involves the integration of multisensory information, including vestibular cues of head motion. Minimizing head motion variability may optimize the information transmitted by vestibular signals that are important for balance control and consequently drive vestibular contributions to locomotion which decrease as we move faster. In this study, participants walked outdoors at 40% to 140% of their preferred step cadence while we characterized head kinematic variability and vestibular-evoked balance responses to electrical vestibular stimulation, a common method to generate virtual signals of head movement. Head kinematic variability was lowest near participants' preferred step cadences (90–126 steps/min) and gait speeds (1.1–1.7 m/s) while vestibular-evoked responses decreased exponentially as step cadence and gait speed increased. Hence, the minima of head kinematic variability were close to preferred step cadences, near previously established minima for the metabolic cost of locomotion. The relationship between head kinematic variability and vestibular-evoked balance responses, however, was inconsistent across all step cadences, suggesting that head kinematic variability did not drive vestibular-evoked balance response magnitude. The observed reduction in the variability of head motion signals at the preferred locomotor cadence/speed may serve to improve our self-motion estimates and reduce information processing requirements to ensure effective navigation, thereby potentially contributing to the well-established minimum in metabolic cost near preferred cadence.

Uncertainty is always present in the sensory information that we receive, worsening confidence in our self-motion estimates. The vestibular system, responsible for detecting head motion in space, provides movement information to our brain, but the certainty of this information is diminished by the inherent noisiness and delays of the neural pathways associated with the encoding of head self-motion cues[1]. As our internal estimate of head motion in space contributes to whole-body balance responses for maintaining our bipedal posture[2,3], it is critical we maximize the reliability of the vestibular signals of head motion when navigating our environment. Similar to how we walk at speeds that minimize our energy expenditure[4–6], it may be beneficial to reduce the uncertainty of the vestibular information given that sensory noise increases the metabolic cost of neuronal information processing[7]. There is evidence that humans minimize head movement variability during locomotion and other complex movements[8–11]. It is not clear, however, if this relates to the task-dependent modulation in the vestibular control of balance during locomotion, an important consideration given the vestibular contributions to maintaining our upright posture as we move.

Clinical and experimental studies have shown that vestibular contributions to balance decrease as locomotor speed and step cadence increase[12–15]. MacNeilage & Glasauer[16] developed a model based on an index of head kinematic variability across strides (V_{res}) that they proposed represents a ratio between motor efference copy noise and vestibular information noise to predict the context-dependent attenuation in the measured vestibular control of balance during locomotion. Their model was inspired by observations in tadpoles and juvenile frogs

[1]School of Kinesiology, University of British Columbia, Vancouver, BC, Canada. [2]School of Biomedical Engineering, University of British Columbia, Vancouver, BC, Canada. [3]Centre for Hip Health and Mobility, University of British Columbia, Vancouver, BC, Canada. [4]Djavad Mowafaghian Centre for Brain Health, University of British Columbia, Vancouver, BC, Canada. [5]Institute for Computing, Information and Cognitive Systems, University of British Columbia, Vancouver, BC, Canada. ✉email: jean-sebastien.blouin@ubc.ca

where contributions of vestibular gaze stabilizing mechanisms decrease and are replaced by feedforward control from the motor efference copy as locomotor speed increases[17–19]. For example, as vestibular noise increases relative to motor noise (i.e., decreased V_{res}), it is predicted that vestibular signals would be downregulated for self-motion estimation, and the magnitude of vestibular balance responses would decrease. Recently, Mackrous and colleagues[20] found no difference in vestibular afferent signals encoding head motion between locomotor speeds in adult nonhuman primates, questioning the presence of peripheral feedforward mechanisms to regulate the vestibular contributions to balance during locomotion in mammals. While human experimental results have shown that V_{res} decreases concurrently with the magnitude of vestibular-evoked balance responses[21,22], this has only been characterized at locomotor speeds (0.4 and 0.8 m/s) and step cadences (52 and 78 steps/minute) slower than our preferred locomotor speed and cadence. Thus, it is critical that we investigate head kinematics and vestibular balance control across a wide range of speeds and cadences given that this relationship may change as speed and cadence increase beyond our preferred movement parameters.

The objective of this study was to characterize the relationship between head kinematic variability and vestibular-evoked balance responses across step cadences representing 40% to 140% of participants' preferred step cadences. Here, we defined head kinematic variability as a ratio of the variability around a stride-cycle attractor representing the average stride head kinematics (residual variability) and the variability around the total average head kinematics within and across strides (i.e., the near zero offset; total variability)[16]. To do so, we used a portable, inertial measurement unit (IMU)-based system (Fig. 1) that can simultaneously apply electrical vestibular stimulation (EVS; a common technique to elicit vestibular-evoked balance responses) and measure kinematics to characterize head movement during locomotion and quantify the magnitude of the EVS-evoked balance responses[22]. Given previous observations, we hypothesized that vestibular-evoked balance responses would decrease as cadence increased past the participants' preferred cadence. It was unclear, however, how head kinematic variability would change for these larger locomotor speeds and cadences. If head variability is minimal at the preferred locomotor cadence, we would expect V_{res} to decrease up to a participant's preferred cadence but to increase beyond the preferred cadence (minima hypothesis). Alternatively, V_{res} may continue to decrease

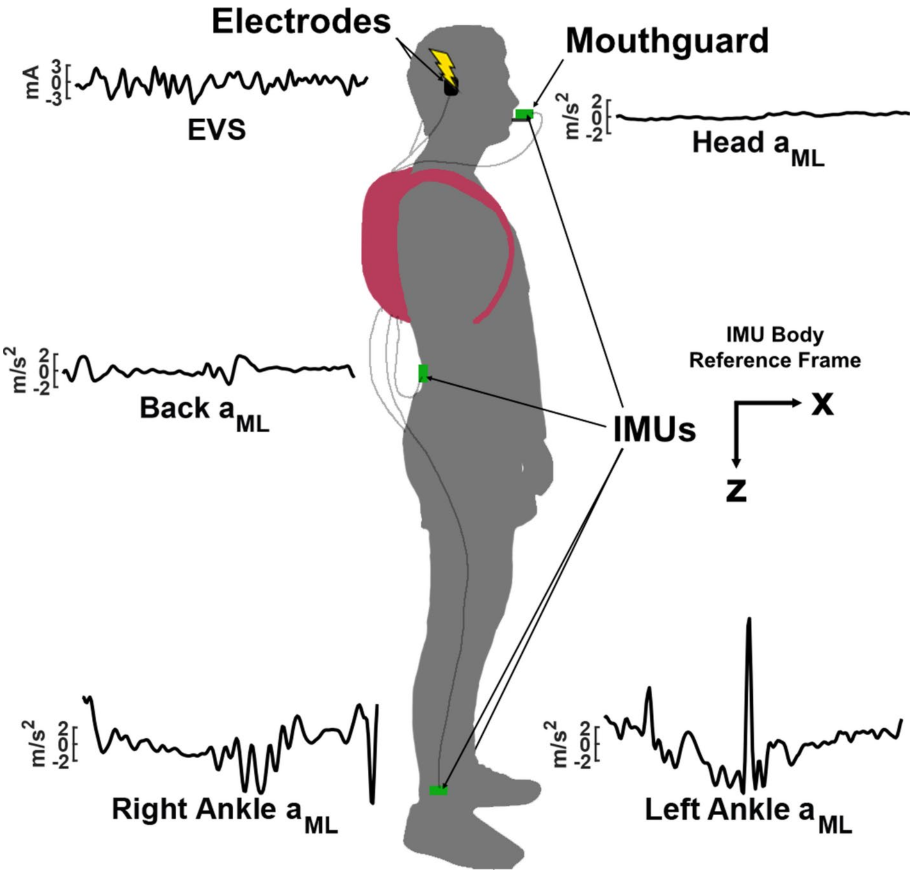

Fig. 1. Diagram of experimental set-up with a participant in a neutral pose. The inertial measurement units (IMUs) and their protective backings were 19.8 mm wide, 15.1 mm tall, and 4.2 mm thick. The backpack contained the myRIO-1900, stimulator, and battery which combined weighed approximately 1.8 kg. The IMU body reference frame was not a global reference frame. Here, it is presented as oriented while the participant is in a neutral pose but would move with the local body segment orientation. Raw traces of the applied electrical vestibular stimulation (EVS) and mediolateral linear accelerations (a_{ML}) from the IMUs are shown for a single stride of a representative participant walking at 63 steps/min and 0.70 m/s. mA, milliamperes; m/s^2, metres per second squared.

beyond the preferred cadence (monotonic decrease hypothesis). A monotonic decrease in V_{res} would support the hypothesis by MacNeilage and colleagues[16] that changes to V_{res} explain the modulation in vestibular-evoked responses.

Results

Twelve healthy young participants completed bouts of walking at 40%, 60%, 80%, 100%, 120%, and 140% of their preferred step cadence. To capture participants' natural locomotor patterns, all walking trials were completed outdoors on a paved surface. We first recorded 30 s of natural walking without EVS to determine the natural step cadence of each participant. At each cadence condition, participants completed 85 strides without EVS followed by 215 strides while experiencing EVS (Methods). EVS modulates the firing rate of primary vestibular nerve afferents via the application of a small electrical current to the mastoid processes, thus eliciting whole-body balance responses of vestibular origin[23]. We estimated head kinematic variability using V_{res}, which is a ratio between the residual variability and total variability of head kinematics across strides (see insets of Figs. 2 and 3 for illustrations of V_{res} calculations, and Eqs. 7–9 in Methods)[16]. Given that the changes to V_{res} across step cadences were similar in the EVS and non-EVS conditions (although the V_{res} was generally ~ 11–23% higher in the trials with EVS; see Supplementary Materials), only the V_{res} data from the trials with EVS are presented here to allow for direct comparison with the vestibular-evoked balance responses. Gait events (heel strike and toe off) were determined using IMUs on each ankle (Methods). Across participants, the preferred step cadence was 107.3 ± 9.1 steps/minute with a resulting gait speed of 1.4 ± 0.3 m/s. From 40 to 140% of the participants' preferred step cadence, step cadence and gait speed increased (43.8 ± 3.8 to 149.4 ± 13.2 steps/min and 0.4 ± 0.1 to 2.1 ± 0.4 m/s, respectively), while the proportion of double leg stance (i.e., the time between right heel strike and left toe-off and the time between left heel strike and right toe-off) decreased, similar to previous observations[24–26] (see Supplementary Materials for complete gait characteristics table). Head orientation,

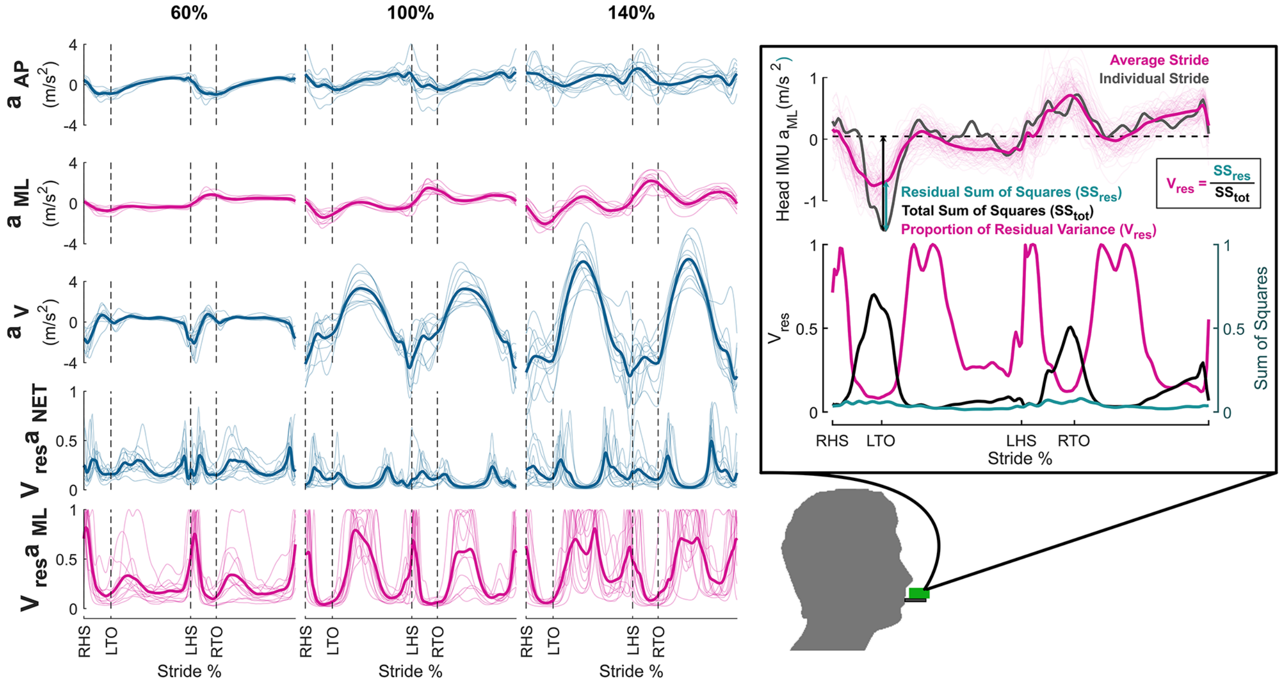

Fig. 2. Group and individual (n = 12) stride-averaged head linear accelerations and related proportion of residual variance (V_{res}) measures for the 60% (left column), 100% (middle column), and 140% (right column) cadence conditions. Thick solid lines represent the mean across participants and thin transparent lines represent the mean from each participant. Right side panel illustrates how the $V_{res}a_{ML}$ was calculated for a single participant at the 60% step cadence condition. For each stride, the squared difference from the average stride cycle kinematics (pink line in top of panel; i.e., stride-cycle attractor) was calculated and the average was taken across all strides, resulting in the residual sum of squares (SS_{res}; light blue line in the panel). Similarly, the squared difference from the average kinematics across and within strides (dashed horizontal grey line; i.e., a single value) was calculated for each stride, and the average across each stride was taken to determine the total sum of squares (SS_{tot}; black line). For net V_{res} calculations (not shown here), the squared differences were also summed across the three dimensions prior to the averaging across strides to calculate SS_{res} and SS_{tot}. V_{res}(pink line in bottom of panel) was then calculated as the ratio between SS_{res} and SS_{tot} for each point of the stride cycle. a_{AP}, anteroposterior linear acceleration (x-axis); a_{ML}, mediolateral linear acceleration (y-axis); a_V, vertical linear acceleration (z-axis); a_{NET}, net linear acceleration; m/s, meters per second squared; RHS, right heel strike; LTO, left toe-off; LHS, left heel strike; RTO, right toe-off.

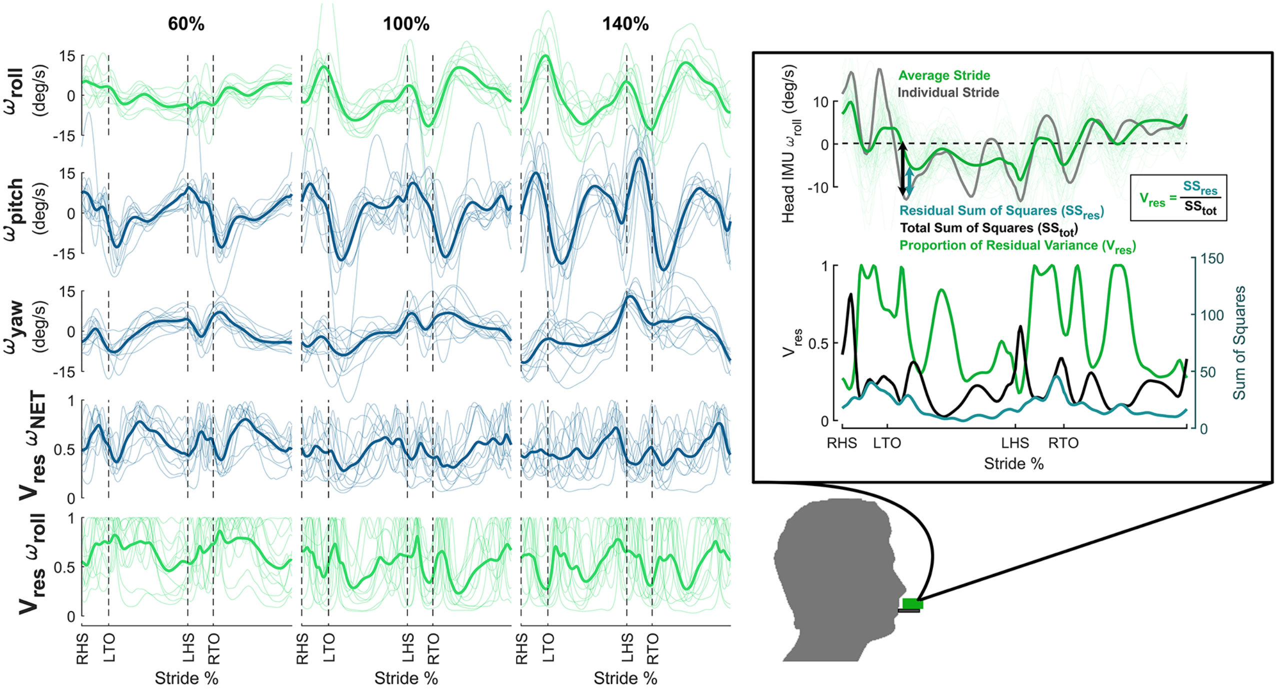

Fig. 3. Group and individual (n = 12) stride-averaged head angular velocities and related proportion of residual variance (V_{res}) measures for the 60% (left column), 100% (middle column), and 140% (right column) cadence conditions. Thick solid lines represent the mean across participants and thin transparent lines represent the mean from each participant. Right side panel illustrates how the $V_{res}\omega_{roll}$ was calculated for a single participant at the 60% step cadence condition. For each stride, the squared difference from the average stride cycle kinematics (green line in top of panel; i.e., stride-cycle attractor) was calculated and the average was taken across all strides, resulting in the residual sum of squares (SS_{res}; light blue line in the panel). Similarly, the squared difference from the average kinematics across and within strides (dashed horizontal grey line; i.e., a single value) was calculated for each stride, and the average across each stride was taken to determine the total sum of squares (SS_{tot}; black). For net V_{res} calculations (not shown here), the squared differences were also summed across the three dimensions prior to the averaging across strides to calculate SS_{res} and SS_{tot}. V_{res}(green line in bottom of panel) was then calculated as the ratio between SS_{res} and SS_{tot} for each point of the stride cycle. ω_{roll}, roll angular velocity (x-axis); ω_{pitch}, pitch angular velocity (y-axis); ω_{yaw}, yaw angular velocity (z-axis); ω_{NET}, net angular velocity; deg/s, degrees per second; RHS, right heel strike; LTO, left toe-off; LHS, left heel strike; RTO, right toe-off.

measured with an IMU fixed to a mouthguard (Methods), changed slightly across the different conditions, with the average head pitch ranging from the lowest at the 40% condition (Reid's plane 4.0 ± 6.1° up from horizontal) to the highest at the 100% condition (8.8 ± 6.4°).

Head kinematics across cadences

To determine stride-by-stride head kinematic variability, we calculated V_{res} using the gravity-corrected and transformed net linear acceleration ($V_{res}\ a_{NET}$), mediolateral linear acceleration ($V_{res}\ a_{ML}$; Fig. 2), net angular velocity ($V_{res}\ \omega_{NET}$), and roll angular velocity ($V_{res}\ \omega_{roll}$; Fig. 3) from a mouthguard-fixed IMU (see Methods; similar to previous work from MacNeilage and Glasauer[16]). $V_{res}\ a_{NET}$ and $V_{res}\ \omega_{NET}$ provide indices of the overall head variability as they are calculated from the linear accelerations and angular velocities from all three axes, respectively. $V_{res}\ a_{ML}$ and $V_{res}\ \omega_{roll}$ are calculated from mediolateral linear acceleration and roll angular velocity, respectively, which correspond to the plane in which the EVS-evoked balance responses occur. We generally observed four peaks of variable amplitude within the stride cycle, corresponding to the approximate locations of heel strikes and toe-offs from both feet. From the 40% to 100% cadence conditions, the mean V_{res} decreased for all participants in all measures except $V_{res}\ a_{ML}$(observed in 10/12 participants). From the 100% to 140% conditions, the mean V_{res} generally increased ($V_{res}a_{NET}$: 9/12 participants; $V_{res}a_{ML}$: 9/12 participants; $V_{res}\omega_{NET}$: 6/12 participants; $V_{res}\omega_{roll}$: 6/12 participants).

We performed repeated measures analysis of variance (rmANOVA) to determine if there was a main effect of step cadence on each measure of head kinematic variability (V_{res}; Table 1 and Fig. 4). Post-hoc paired Student t-tests ($\alpha = 0.05$) were performed between the following step cadence conditions: 40–100% to confirm that V_{res} decreased[21,22] up to the preferred cadence (one-tailed), and 100–120% and 100–140% to characterize how head kinematic variability changed beyond the preferred cadence (two-tailed). To correct for multiple comparisons, we used the Holm method. For all V_{res} measures, we observed significant main effects and a significant decrease

Measure	rmANOVA F-statistic	p	Post-hoc Student t-test	t-statistic	Cohen's d	p_{holm}
$V_{res}a_{NET}$	$F_{1.910,21.015}=93.871$	**<0.001**	40 vs 100%	$t_{11}=20.208$	5.834	**<0.001***
			100 vs 120%	$t_{11}=-1.151$	−0.335	0.270
			100 vs 140%	$t_{11}=-2.821$	−0.814	**0.034†**
$V_{res}a_{ML}$	$F_{2.345,25.798}=15.063$	**<0.001**	40 vs 100%	$t_{11}=4.009$	1.157	**0.003***
			100 vs 120%	$t_{11}=-2.719$	−0.785	**0.020†**
			100 vs 140%	$t_{11}=-3.339$	−0.964	**0.014†**
$V_{res}\omega_{NET}$	$F_{2.017,22.188}=31.304$	**<0.001**	40 vs 100%	$t_{11}=8.939$	2.580	**<0.001***
			100 vs 120%	$t_{11}=1.363$	0.393	0.400
			100 vs 140%	$t_{11}=-0.472$	−0.136	0.646
$V_{res}\omega_{roll}$	$F_{1.652,18.176}=13.583$	**<0.001**	40 vs 100%	$t_{11}=6.950$	2.006	**<0.001***
			100 vs 120%	$t_{11}=0.543$	0.157	1.000
			100 vs 140%	$t_{11}=-0.584$	−0.169	0.571

Table 1. Statistical analysis of the mean proportion of residual variance (V_{res}) calculated from the gravity-corrected and transformed net linear acceleration ($V_{res}a_{NET}$), mediolateral linear acceleration ($V_{res}a_{ML}$), net angular velocity ($V_{res}\omega_{NET}$), and roll angular velocity ($V_{res}\omega_{roll}$). These measures were calculated from trials where vestibular stimulation was applied. A repeated measures analysis of variance (rmANOVA) was performed for each measure, along with selected post-hoc Student t-tests (corrected with Holm method). Significant results are indicated with boldface type and an asterisk (*) denotes a significant decrease while a dagger (†) denotes a significant increase.

from the 40% to 100% step cadence condition (0.24–0.72 ×; Table 1). In contrast, we observed significant increases from the 100% to 140% condition in the mean $V_{res}a_{NET}$(1.59 ×; Table 1), and from 100 to 120% and 140% in the mean $V_{res}a_{ML}$(1.22–1.37 ×; Table 1). There were no significant changes in the V_{res} ω_{NET} or V_{res} ω_{roll} beyond the 100% step cadence condition.

Vestibular responses across cadences

We also calculated the time-dependent coherence between EVS and kinematic signals (i.e., a measure of relation between two signals; see Methods) for each individual participant and across all participants to quantify the magnitude of vestibular-evoked balance responses[27,28]. Larger coherence values indicate stronger relation between vestibular input and balance responses, thus calculating coherence across cadences allowed us to quantify changes in vestibular-evoked responses as a function of step cadence. Gain was also calculated (see Supplementary Materials), but only coherence is presented here as the changes in gain between step cadences were similar to and supported the coherence results. Time-dependent coherence was calculated between the EVS and the gravity-corrected and transformed mediolateral (ML) linear accelerations from IMUs placed on the low back and each ankle. This allowed us to characterize the vestibular-evoked balance responses at the approximate centre of mass and in the lower limbs, respectively. We observed regions of significant coherence (based on a 99% confidence limit) in all participants and IMUs in the 40–100% cadence conditions (see Fig. 5 for representative participant). Significant coherence was generally observed between 0–10 Hz during single-leg stance in the back and during stance phases in the corresponding ankles, similar to previous findings[22]. All participants exhibited significant coherence in the 120% condition for all IMUs, except for one participant's left ankle ML accelerations. For the 140% cadence condition, we observed significant coherence in 9/12 participants for the back ML acceleration and 11/12 participants for the right and left ankle ML accelerations.

We extracted the peak coherence from across the stride cycle and frequencies and performed rmANOVAs to determine if there was a main effect of step cadence on peak coherence (Table 2 and Fig. 6). To confirm that the vestibular-evoked responses decreased in magnitude with increasing step cadence, the following post-hoc, one-sided paired Student t-tests were performed: 40–100% to confirm previous findings, and 100–120% and 100–140% to verify that the vestibular responses decreased in magnitude beyond the preferred step cadence. We observed significant main effects for all coherence measures (back, right ankle, and left ankle ML linear accelerations). Additionally, we observed significant decreases in all post-hoc t-tests (40–100%: 0.27–0.34 ×, 100–120%: 0.59–0.64 ×, 100–140%: 0.31–0.46 ×; Table 2), except from the 100% to 120% condition in the back ML linear acceleration peak coherence.

To directly relate V_{res} and coherence, we determined linear fits and calculated the coefficient of determination (R^2) of the linear fits between each combination of mean V_{res} and peak coherence measures. This was calculated for all step cadence conditions, 40% to 100% step cadence conditions, and the 100% to 140% step cadence conditions. While there was a positive relationship between V_{res} and coherence from 40 to 100%, the relationship was negative or zero from 100 to 140%. Furthermore, in all cases (except the linear fits between V_{res} ω_{roll} and left ankle peak coherence), the R^2 decreased when fitting data from the 40% to 100% conditions compared to data from all step cadences. Consequently, the linear fits worsened when the faster step cadences were added. We presented only the linear fits with the peak back coherence in Fig. 4 because all coherence measures yielded similar results. The linear fits with all other coherence measures are included in the Supplementary Materials.

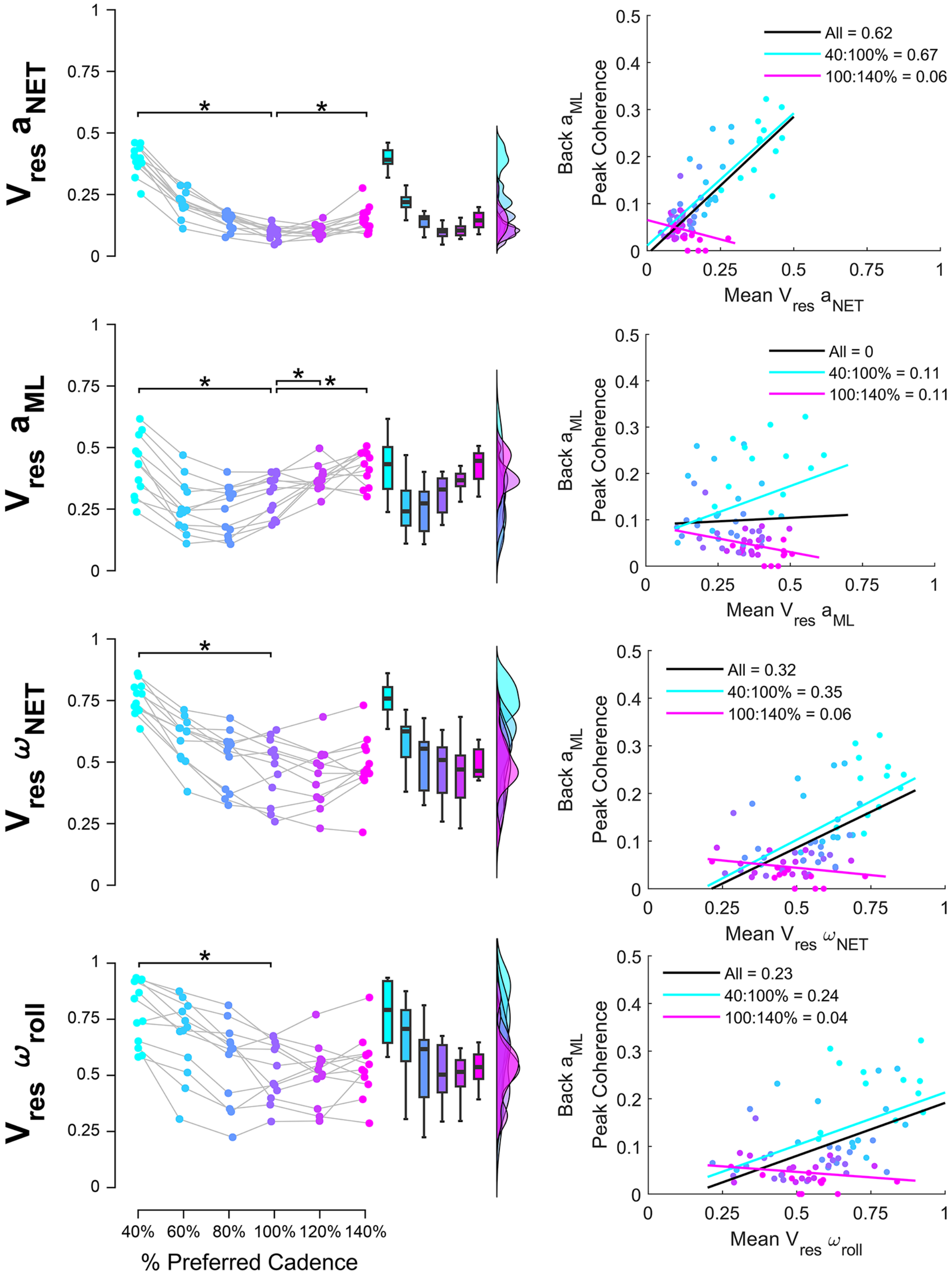

Fitting head kinematics and vestibular changes across step cadence and gait speed

To establish the relationship between head kinematic variability and vestibular-evoked balance responses with step cadence and gait speed, we fitted functions to mean V_{res} and peak coherence, respectively.

Head kinematic variability

We fitted both 2nd degree polynomial (minima hypothesis) and exponential decay (monotonic decrease hypothesis) functions to the mean V_{res} measures from all participants. The difference in the Akaike information criterion (AIC) between the polynomial and decay fits (ΔAIC = polynomial – exponential decay) was calculated to identify the most appropriate fit (a lower AIC indicates a more appropriate model; see Methods). If $\Delta AIC > 0$, the exponential decay was the most appropriate fit and if $\Delta AIC < 0$, the polynomial was the most appropriate fit. Using the fitting method that best represented the group data, we then fitted each participant's individual data and calculated the adjusted coefficient of determinations ($\overline{R}^2$). The AIC was lower in the polynomial fits compared to the exponential decay fits for head kinematic variability across step cadences ($V_{res}a_{NET}$:$\Delta AIC = -78.5$, polynomial $\overline{R}^2 = 0.94 \pm 0.05$; $V_{res}a_{ML}$: $\Delta AIC = -40.2$, polynomial

◂**Fig. 4**. Participant (n = 12) mean proportion of residual variance (V_{res}) across step cadence conditions during trials *with electrical vestibular stimulation* (left column) and linear fits between mean V_{res} and back mediolateral linear acceleration (a_{ML}) coherence (right column). We calculated V_{res} with the head net linear acceleration ($V_{res}a_{NET}$), mediolateral linear acceleration ($V_{res}a_{ML}$), net angular velocity ($V_{res}\omega_{NET}$), and roll angular velocity ($V_{res}\omega_{roll}$). There was a significant main effect for all V_{res} measures. Post-hoc t-test revealed that there was a significant decrease from the 40% to 100% step cadence condition for all measures. Increases were only observed between the 100–140% comparison for the $V_{res}a_{NET}$ as well as between the 100–120% and 100–140% comparisons for the $V_{res}a_{ML}$. For the linear fits (right column) between the mean V_{res} measures and peak back coherence, the legend indicates the coefficient of determination (R^2) for the linear fit with all the step cadence conditions ("All", black), the linear fit with the 40% to 100% step cadence conditions ("40:100%", light blue), and the linear fit with the 100% to 140% step cadence conditions ("100:140%", pink). In all cases shown, 40–100% fit and the 100–140% were near orthogonal and the R^2 was lower in the linear fit with all conditions compared to the linear fit with the 40% to 100% conditions. Closed circles represent the values from individual participants. Boxplots represent the median and interquartile range of the data. * denotes statistically significant differences between conditions from post-hoc t-tests ($p < 0.05$).

$\overline{R}^2 = 0.35 \pm 0.65$; V_{res} ω_{NET}: $\Delta AIC = -41.3$, polynomial $\overline{R}^2 = 0.83 \pm 0.19$; V_{res} ω_{roll}: $\Delta AIC = -13.6$, polynomial $\overline{R}^2 = 0.78 \pm 0.19$; Fig. 7A) and gait speeds ($V_{res}a_{NET}$: $\Delta AIC = -69.3$, polynomial $\overline{R}^2 = 0.86 \pm 0.20$; $V_{res}a_{ML}$: $\Delta AIC = -39.9$, polynomial $\overline{R}^2 = 0.20 \pm 0.67$; $V_{res}\,\omega_{NET}$: $\Delta AIC = -64.9$, polynomial $\overline{R}^2 = 0.71 \pm 0.32$; $V_{res}\,\omega_{roll}$: $\Delta AIC = -38.4$, polynomial $\overline{R}^2 = 0.71 \pm 0.25$; Fig. 7B).

To determine the locomotor cadence and speed at which head kinematic variability was minimal, we extracted the minimum value for each participant's 2nd degree polynomial function. The locations of the minima varied between 90–126 steps/min across step cadences ($V_{res}a_{NET}$ at 117 ± 9 steps/min; $V_{res}a_{ML}$ at 90 ± 17 steps/min; $V_{res}\,\omega_{NET}$ at 126 ± 16 steps/min; $V_{res}\,\omega_{roll}$ at 125 ± 25 steps/min; Fig. 7A) and 1.1–1.7 m/s across gait speeds ($V_{res}a_{NET}$ at 1.5 ± 0.2 m/s; $V_{res}a_{ML}$ at 1.1 ± 0.3 m/s; $V_{res}\,\omega_{NET}$ at 1.7 ± 0.2 m/s; $V_{res}\,\omega_{roll}$ at 1.7 ± 0.3 m/s; Fig. 7B).

Vestibular-evoked balance responses

To confirm that vestibular-evoked balance responses decreased with step cadence, we fitted exponential decay functions to each individual participant's peak coherences from the three IMU measurements. In general, the exponential decay functions were well fitted to the data as demonstrated by the large $\overline{R}^2$ values (back: 0.90 ± 0.06; right ankle: 0.85 ± 0.14; left ankle: 0.86 ± 0.18; Fig. 8A). We found similar results when fitting the peak coherences across gait speeds (back: 0.89 ± 0.07; right ankle: 0.84 ± 0.15; left ankle: 0.87 ± 0.17; Fig. 8B).

Discussion

We found that, contrary to the model proposed by MacNeilage and colleagues, head kinematic variability did not predict vestibular modulations at step cadences faster than 100% of preferred cadence. To determine this, we measured V_{res}, a metric of head kinematic variability across strides, and EVS-evoked balance responses from participants as they walked at cadences ranging from 40 to 140% of their natural step cadence in the real-world. Across all the V_{res} measures computed, a 2nd degree polynomial function, with the minimum near the preferred step cadences, fitted the data better than an exponential decay function. In contrast, the peak magnitude of the vestibular-evoked balance responses decreased as step cadence increased and was well fitted to an exponential decay function as hypothesized. These results suggest that head kinematic variability is minimal near our preferred locomotor cadences and is not the driving factor in the cadence and speed induced modulation of vestibular balance control.

Head kinematic variability is minimal near preferred step cadences

The changes to head kinematic variability (V_{res}) across step cadences and gait speeds were best fitted to 2nd degree polynomial curves. The local minima in polynomials fitted to the mean V_{res} were located at 90–126 steps/min and 1.1–1.7 m/s across step cadence and gait speed, respectively. These correspond with the range of step cadences (96–126 steps/min) and gait speeds (0.9–1.8 m/s) that we identified during the preferred cadence condition and is similar to what has previously been measured as preferred step cadences and gait speeds[29–34]. Hirasaki et al.[9] found that within the gait speed range of 1.2–1.8 m/s (and step cadences of 108–132 steps/min), head and body coordination was optimized, and the bandwidth around the predominant frequency of the vertical translation spectral density was minimized. This speed range is also optimal for minimizing energetic cost during locomotion[35,36]. Furthermore, other authors have observed that the symmetry of head movement is optimized at preferred step cadences and speeds, which they argued reflects head stability[30,31]; although we note that this interpretation has been criticized[37,38].

MacNeilage and Glasauer[16] proposed that V_{res}, which is calculated as the ratio of residual to total head kinematic variability over a stride cycle, represents a ratio of the motor noise to the proportion of sensory (vestibular) noise. However, an alternative interpretation of V_{res} is that it represents a "noise-to-signal" ratio of the head kinematics, rather than a predictor of vestibular-evoked balance responses. In this view, the variance of the head movement signals around the mean across stride cycles (i.e., the numerator of the V_{res} equation) is considered the sensory noise which is then compared to the overall signal amplitude (as measured by the total sum of squares, i.e., the denominator of the V_{res} equation). Unlike the previous interpretation, this does

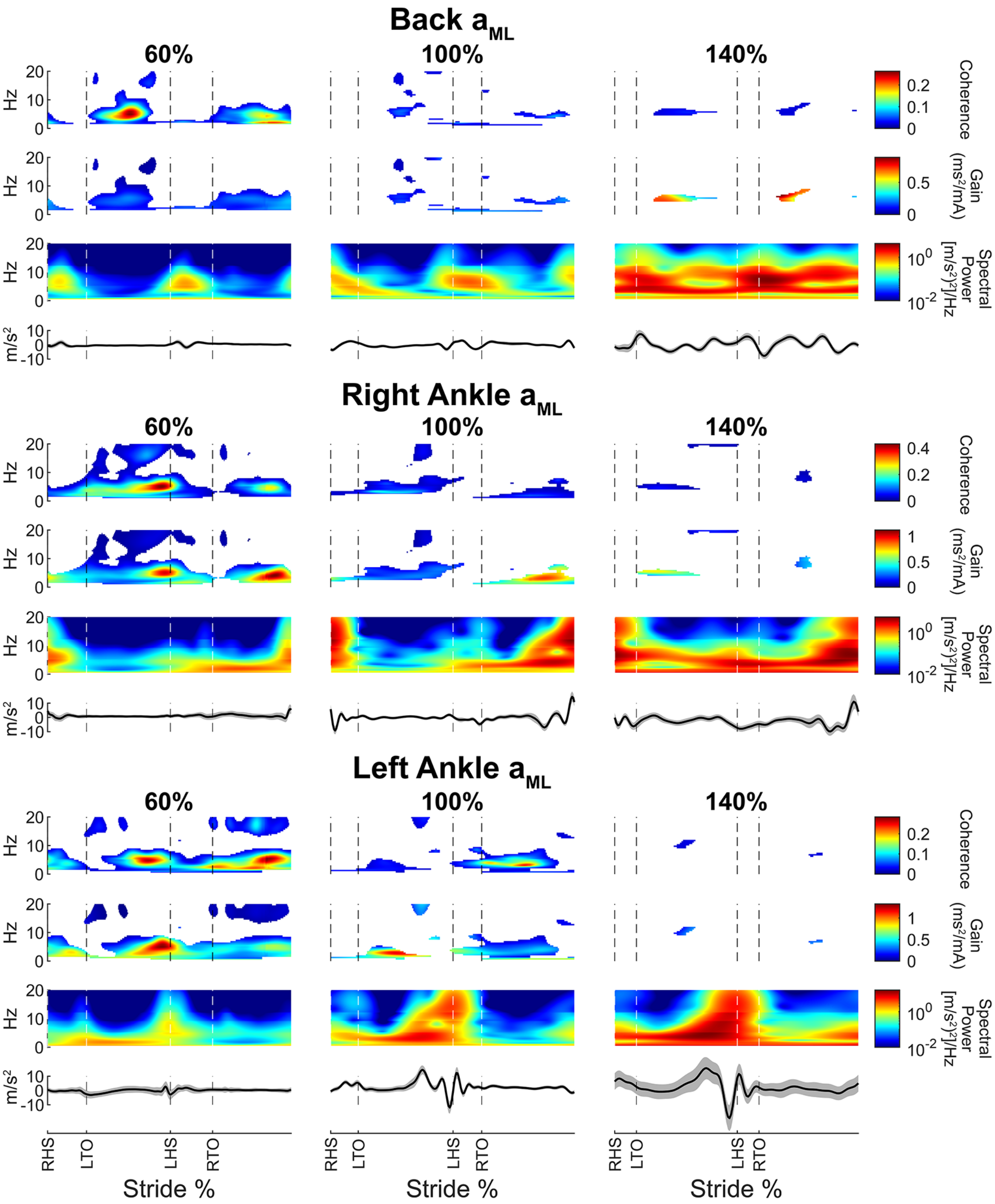

Fig. 5. Representative participant time-dependent frequency representations shown at 60% (left column), 100% (middle column), and 140% (right column) of their preferred cadence. For each sensor, the coherence (1st row), gain (2nd row), spectral output power (3rd row), and time traces (4th row; mean: solid line, standard deviation: shaded area) are presented. We calculated coherence and gain between the applied electrical vestibular stimulation and the back mediolateral linear acceleration (a_{ML}; top), right ankle a_{ML}(middle), and left ankle a_{ML}(bottom). Values representing non-significant coherence and gain were removed from the plots. Spectral output power was calculated with the a_{ML} from each sensor. Significant coherence was generally observed during single-leg stance in the back and during stance phase in the ankles. At the slow cadences, gain followed a similar pattern; however, gain was more inconsistent at faster cadences due to the low coherence. Spectral output power generally increased with step cadence, especially at heel strikes. mA, milliamperes; m/s^2, metres per second squared; RHS, right heel strike; LTO, left toe-off; LHS, left heel strike; RTO, right toe-off.

not depend on the assumption of Weber's law that signal amplitude is proportional to sensory noise[39], which may not be followed for vestibular cues of self-motion[40,41]. Given this interpretation, our results suggest that the vestibular "noise-to-signal" ratio is minimal near our preferred cadences and gait speeds.

There is evidence that greater noise in sensory signals increases the metabolic cost of neuronal information processing[7] and that this information processing is optimized to reduce metabolic cost[42]. Thus, reducing the variability of our head movement may serve to minimize the energy requirements of processing vestibular

Measure	rmANOVA F-statistic	p	Post-hoc Student t-test	t-statistic	Cohen's d	p_{holm}
Back a_{ML}	$F_{2.178,23.956} = 55.741$	**< 0.001**	40 vs 100%	$t_{11} = 9.529$	2.751	**< 0.001***
			100 vs 120%	$t_{11} = 1.006$	0.291	0.168
			100 vs 140%	$t_{11} = 3.807$	1.099	**0.002***
Right ankle a_{ML}	$F_{2.762,30.377} = 41.956$	**< 0.001**	40 vs 100%	$t_{11} = 9.629$	2.780	**< 0.001***
			100 vs 120%	$t_{11} = 2.231$	0.644	**0.024***
			100 vs 140%	$t_{11} = 3.036$	0.884	**0.010***
Left ankle a_{ML}	$F_{5,55} = 51.776$	**< 0.001**	40 vs 100%	$t_{11} = 11.590$	3.346	**< 0.001***
			100 vs 120%	$t_{11} = 1.902$	0.549	**0.042***
			100 vs 140%	$t_{11} = 3.338$	0.964	**0.006***

Table 2. Statistical analysis of the peak coherence calculated between the electrical vestibular stimulation and the gravity-corrected, mediolateral linear accelerations (a_{ML}) from the back, right ankle, and left ankle. A repeated measures analysis of variance (rmANOVA) was performed for each measure, along with selected post-hoc Student t-tests (corrected with Holm method). Tests were performed on Fisher transformed coherence values. Significant results are indicated with boldface type and an asterisk (*) denotes a significant decrease.

information. Given the large energy demands of the central nervous system and evolutionary pressures to optimize energy expenditure and the quality of sensory information encoded[43,44], our preferred movement patterns may have evolved to balance between the energetic costs of our motor commands and the central sensory information processing pressures of signal quality, metabolic cost, and number of neurons required. For example, it has been shown that humans choose locomotor patterns that are not energetically optimal when step length and width are constrained[45], suggesting that other factors – possibly head kinematic variability – are important considerations for how we choose our locomotor patterns. Alternatively, given that that blood gas receptors do not sense energetic cost during locomotion[46], it is possible that our head kinematics provide partial (and indirect) information to facilitate energetic optimization during locomotion. These results open the door to future work exploring how the metabolic costs of our motor actions and sensory processing demands are balanced as we navigate our environment.

Head kinematic variability does not modulate vestibular-evoked balance responses

We also characterized the changes to head kinematic variability and vestibular-evoked balance responses at faster step cadences. For the V_{res} measures using the linear head accelerations ($V_{res}\ a_{NET}$ and $V_{res} a_{ML}$), we generally observed that the participant mean V_{res} values increased beyond the 100% cadence condition (except in the 100–120% $V_{res}\ a_{NET}$ comparison). These increases in mean V_{res} ranged from 17–35% between the 100% and 120% conditions, and 39–77% between the 100% and 140% cadence conditions. Given that increased V_{res} was suggested to indicate that sensory noise has decreased relative to motor noise[16], the magnitude of vestibular-evoked balance responses should consequently increase. However, we observed significant decreases (51–60% decrease) in the extracted peak coherences between the 100% and 140% step cadence conditions. While there were no differences detected in the V_{res} measures driven by the angular velocity of the head ($V_{res}\ \omega_{NET}$ and $V_{res}\ \omega_{roll}$), possibly due to the greater variance in the mean V_{res} values extracted for these measures, these measures did not decrease with the vestibular-evoked balance responses. We also observed that the V_{res}-coherence correlations from the 40–100% cadence conditions and the 100–140% conditions were near orthogonal, especially in the linear acceleration V_{res} measures. Furthermore, the correlations between V_{res} and coherence were positive from the 40–100% cadence conditions but not for the 100–140% conditions, indicating that the relationship between V_{res} and coherence was not consistent across step cadences. Previous studies at slower step cadences and gait speeds have observed mean V_{res} decrease 14–51% as step cadence and gait speed increased (at 52 steps/min and 0.4 m/s to 78 steps/min and 0.8 m/s)[21,22]. At the same step cadences and speeds, decreases in the peak coherence between EVS and muscle activity (17–31%)[13], centre of pressure displacement (47%)[21], and linear accelerations (34–38%)[22] have been reported. In accordance with ths previous observations, we found the mean V_{res} decreased by 14–45% between the 40% and 60% step cadence conditions, which corresponded to average step cadences of 44 and 65 steps/min, respectively. Concurrently, we observed decreases (25–32%) in the peak coherence from the back and ankle ML linear acceleration coherence, which approximate respectively the vestibular-evoked responses of the whole-body body centre of mass and individual lower limbs.

To characterize the overall change in vestibular balance control across step cadences and gait speeds, we fitted exponential decay curves to the participant peak coherences. For all IMUs, the exponential decay curve was well suited to represent the decreased magnitude of vestibular-evoked balance responses as a function of step cadence and gait speed. Given that both the paired t-tests and the fitted the exponential decay functions indicated a continued decrease in vestibular-evoked responses, these results complement previous studies measuring vestibular balance responses at slower locomotor cadences while also extending these findings to preferred and faster walking. This supports our hypothesis, as well as observations in clinical studies[12], that the vestibular-evoked balance responses would decrease as step cadence (and gait speed) increased beyond our preferred step cadence. However, the increasing (linear accelerations) or unchanging (angular velocities)

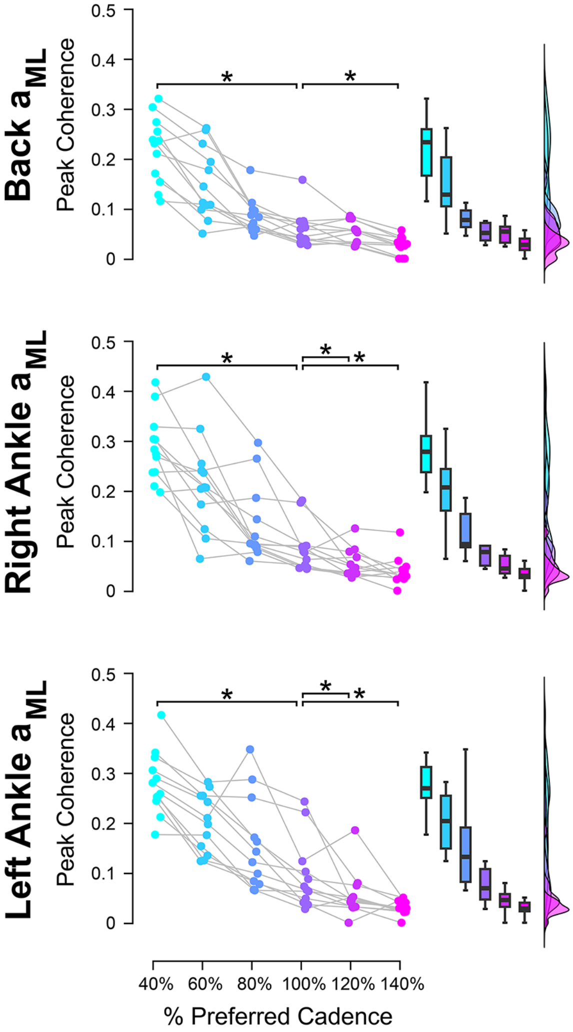

Fig. 6. Peak coherence between EVS and kinematics across step cadences. For each participant ($n = 12$), we calculated peak coherence between the applied electrical vestibular stimulation and the back mediolateral linear acceleration (a_{ML}; top), right ankle a_{ML}(middle), and left ankle a_{ML}(bottom) across step cadences. There was a significant main effect for all coherence measures and a significant decrease in all measures for all post-hoc comparisons (40 vs 100%, 100 vs 120%, and 100 vs 140%), except in the 100 vs 120% comparison for the back a_{ML}. Closed circles represent the peak coherence from individual participants. Boxplots represent the median and interquartile range of the data. * denotes statistically significant differences between conditions from post-hoc t-tests ($p < 0.05$).

V_{res} at faster cadences contradicts the prediction that changes to V_{res} will reflect vestibular balance response modulations at faster step cadences, suggesting that the vestibular control of balance during locomotion is not modulated by the ratio of motor to sensory noise as quantified by V_{res}.

The increased head kinematic variability at faster cadences/speeds does not preclude the proposal by MacNeilage and colleagues that the reduction in vestibular-evoked balance responses at faster step cadences/speeds may be related to a relative increase in the feedforward control of locomotion. Although Mackrous et al.[20] revealed no attenuation of vestibular primary afferents in adult primates during locomotion, suppression of vestibular signals may occur in the vestibular nuclei (see review by Cullen[47]) and be influenced by factors not captured by V_{res}. Alternatively, this modulation of vestibular-evoked balance responses could arise from body stability demands, as providing external pelvis stabilization or increasing step width have been shown to decrease vestibular balance responses during locomotion[48]. Additionally, when walking on a split-belt treadmill, the modulation of the vestibular-evoked responses is consistent with the kinematics from each limb[49]. A direct relation between these vestibular modulations and changes in head kinematic variability, however, cannot be determined given that head kinematics were not recorded in these studies.

Another possible explanation for the attenuation of vestibular balance as cadence increases may be related to non-linearities in vestibular afferent encoding of head motion[20,50] and bi-linear vestibular nuclei gains[51], resulting in saturation of head motion signals. To test if non-linear processes in vestibular pathways contributed to the attenuation of the vestibular evoked balance responses, we modelled the vestibular afferent responses

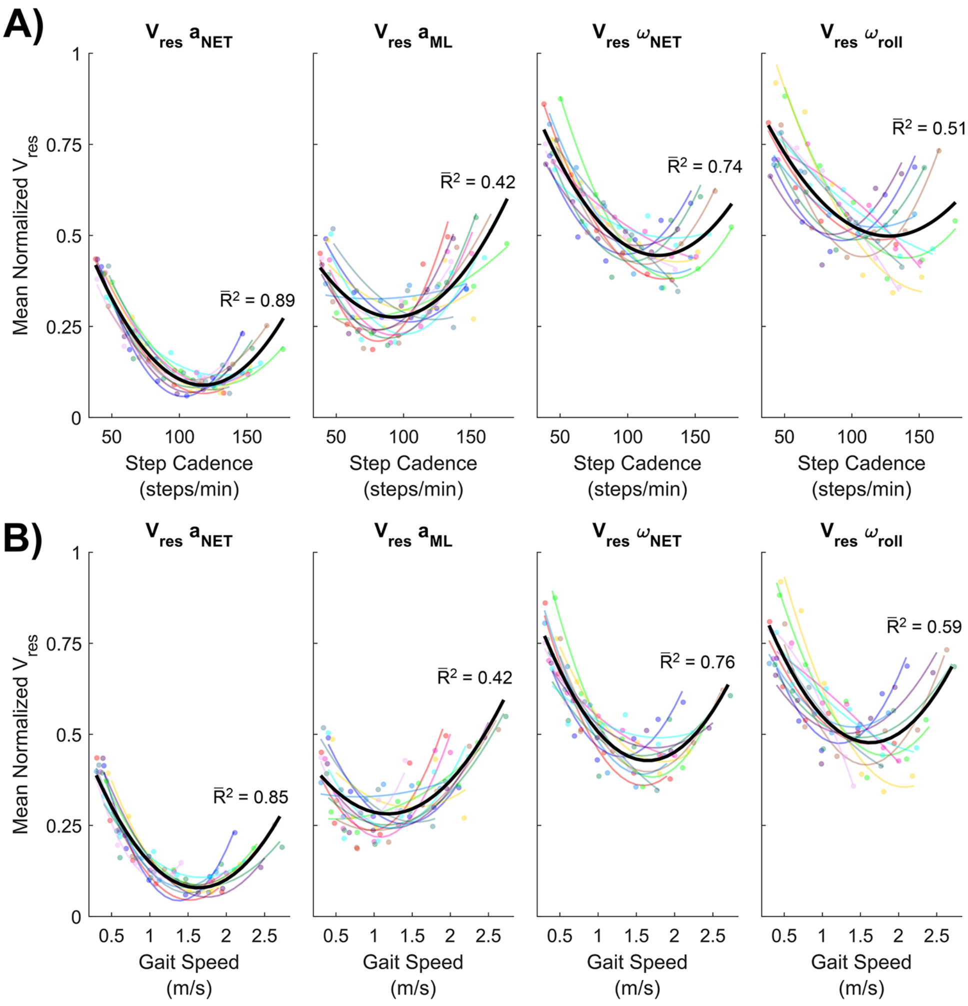

Fig. 7. Participant (n = 12) mean normalized proportion of residual variance (V_{res}) across (**A**) step cadences and (**B**) gait speeds. We calculated V_{res} with the head net linear acceleration ($V_{res}a_{NET}$), mediolateral linear acceleration ($V_{res}a_{ML}$), net angular velocity ($V_{res}\omega_{NET}$), and roll angular velocity ($V_{res}\omega_{roll}$). Individual participant measures and fits are indicated with the same marker and line colour within and across plots. Thick black lines represent the group 2nd degree polynomial fits for each plot with the adjusted coefficient of determination ($\overline{R}^2$) presented. steps/min, steps per minute; m/s, metres per second.

to head motion and electrical stimuli[20,50,52,53] as well as the known vestibular peripheral (sigmoid function to maintain firing rates between 0 and 250 Hz)[20,50] and central (bi-linear gains)[51] non-linearities (see Supplementary Materials). In summary, we found that the predicted vestibular afferent responses generally did not saturate (less than 2% of predicted firing rates occurred outside the 50–200 Hz range), even at the higher step cadences. Consequently, when we calculated coherence between the body kinematics and the simulated central vestibular nuclei firing rates, it was not different than when using the true EVS signal. Thus, it is unlikely that vestibular afferent non-linearities and bi-linear vestibular nuclei gains are responsible for the attenuation of vestibular-evoked balance responses as locomotor cadence and speed increase.

Limitations

As we did not restrict head orientation during trials, participants walked with their head more flexed (pitched down) as their step cadence deviated from the preferred rate (both slower and faster). The observed changes in mean head pitch angle, however, were modest (8.8° to 4.0° up from horizontal). These small head angle changes would be expected to alter the vestibular-evoked responses by 2% if we assume a net EVS vector pointing 17–19° up from Reid's plane[23]. Given that we observed changes ranging from 25–60% between locomotor cadences/speeds, it is unlikely that any head orientation induced change to the EVS-evoked responses had any noticeable effect on our results.

Caution should be exercised when interpreting the lower peak coherence values that we measured at the fastest step cadences. Many of the peak coherence values we extracted at the cadence conditions of 100% and beyond were just higher than the minimum threshold for the individual participant coherence (0.0212). For example, if the coherence confidence limit was increased to 99.9% (increasing the significance threshold by ~ 50%), a larger number of participants would exhibit no coherence at the faster cadences (back: 2 at 100%,

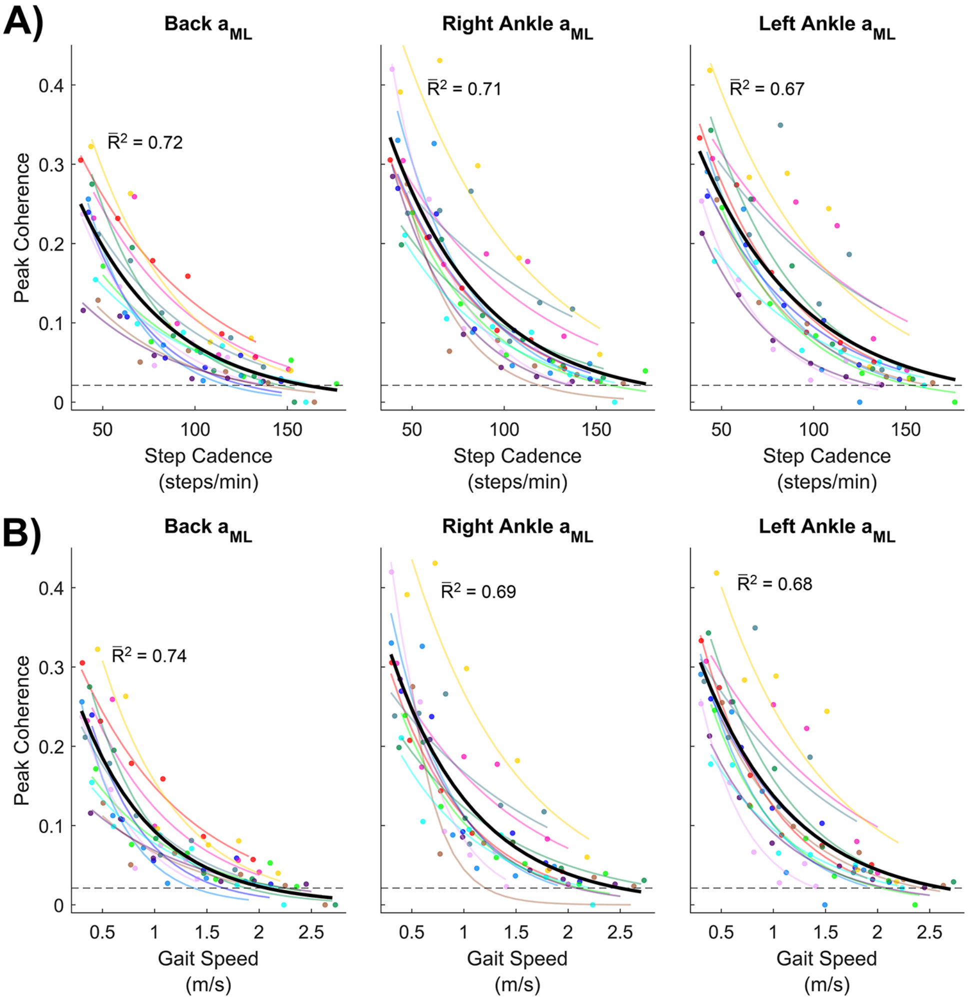

Fig. 8. Participant (n = 12) peak coherence across (**A**) step cadences and (**B**) gait speeds. We calculated coherence between the applied electrical vestibular stimulation and the back, right ankle, and left ankle mediolateral linear accelerations (a_{ML}). Individual participant measures and fits are indicated with the same marker and line colour within and across plots. Thick black lines represent the group exponential decay fits for each plot with the adjusted coefficient of determination ($\overline{R}^2$) presented. Dashed horizontal line indicates threshold for coherence significance (0.0212). steps/min, steps per minute; m/s, metres per second.

3 at 120%, and 7 at 140%; right ankle: 1 at 120% and 7 at 140%; left ankle: 1 at 100%, 2 at 120%, and 8 at 140%) compared to the confidence interval of 99% that we used (back: 3 at 140%, right ankle: 1 at 140%; left ankle: 1 at 120% and 1 at 140%). Upon further inspection, we observed that many of the coherence peaks in the 120% and 140% cadence conditions occurred outside of the typical timing (stance phase) and frequency (0–10 Hz) where coherence was observed. However, it is unlikely that this affected the results and interpretation of our data, given that peak coherences we observed for these conditions were low and would be unlikely to influence the fit of the exponential decay functions.

Conclusion

In summary, we observed that V_{res} was minimal near our preferred cadences and gait speeds while the magnitude of the vestibular-evoked balance responses decreased as step cadence increased. This demonstrates that V_{res} does not predict vestibular responses at faster step cadences and speeds. Furthermore, our results show that head kinematic variability is reduced at preferred step cadences to potentially minimize the cost of processing noisy information in our vestibular sensing. We propose that optimizing sensory information during locomotion decreases the metabolic cost of information processing while improving our internal and perceptual self-motion estimates, making us more effective in navigating our environment.

Methods

Participants

We recruited 14 healthy young adult participants with no neurological or musculoskeletal impairments to participate in this study. However, two were unable to complete the experiment due to discomfort with the EVS so the final sample size consisted of 12 participants. To determine an appropriate sample size, we performed power analyses given effect sizes (1.403–3.009) between the magnitude of vestibular responses observed at 52 steps/min and 78 steps/min[22]. We determined that the minimal sample size for a two-sided paired sample t-test with a desired α = 0.05 and power = 0.9 was 8 participants and we added an additional 4 to account for the smaller differences between step cadences for a total of 12 participants (6 females, 6 males; age = 24.3 ± 2.5 years; height = 171.8 ± 13.4 cm; mass = 71.1 ± 17.0 kg). This experiment was reviewed by the University of British Columbia Clinical Research Ethics Board (H22-01776) and participants provided written informed consent prior to enrolling in the study. All research was performed in accordance with relevant guidelines/regulations and conformed to the declaration of Helsinki, with the exception of registration to a database.

Set-up

Participants were instructed to wear athletic clothing and comfortable running shoes for walking, to replicate their natural walking behaviour. We attached four inertial measurement units (IMUs; MPU 6050; accelerometer range = ± 16 g; gyroscope range = ± 2000˚/s) to the participant for the duration of the experiment (Fig. 1). The first IMU was mounted to a custom-made mouthguard that was prepared for each participant using a vinyl polyciliate putty to form a dental impression and ethylene vinyl acetate to vacuum form the mouthguard. The IMU was mounted on a small cast acrylic tab attached to the mouthguard so that it sat outside the mouth. By fixing the IMU directly to the skull via the upper dentition, we can record head kinematics without skin motion artefact[54]. The second IMU was placed on the low back at the third lumbar spinous process and the height was measured for each participant (105.3 ± 9.6 cm SD). This placement was chosen to approximate the body centre of mass accelerations which we have previously used to characterize whole-body vestibular responses during locomotion[22]. The remaining two IMUs were placed just above each lateral malleolus to detect heel strike and toe-off[55] and characterize lower limb vestibular responses[22,56].

IMU calibration

Each IMU was first calibrated to correct the sensitivity and bias of the accelerometer and the bias in the gyroscopes[57]. We performed IMU-to-body calibration prior to the experimental trials to align the IMUs to a body reference frame with x: forward, y: right, and z: down (Fig. 1). After being attached to the participant, we recorded two 5 s calibration poses for each IMU[58]. The first calibration pose was performed with the participant standing upright, to define the true z-axis. For the head IMU, this involved levelling the head so that Reid's plane was perpendicular to gravity to orient the head IMU with respect to the vestibular apparatus. Then, the participant pitched each respective body segment ~ 90 degrees forward to define an approximate x-axis for the second calibration position. The approximate x-axis and true z-axis were defined as opposite to the net acceleration vector caused by the gravitational field. The true y-axis was calculated as the cross-product of the true z-axis and the approximate x-axis. Finally, the true x-axis was calculated as the cross-product between the true y-axis and the true z-axis.

Portable system

We previously devised a portable system for concurrent kinematic measurement and electrical stimulation, employing a reconfigurable I/O device (myRIO-1900, National Instruments) equipped with a field-programmable gate-array running LabVIEW 2019b (National Instruments)[22]. In this setup, the microcontroller communicated to each of the IMUs with I^2C protocol via a wired connection. An analog output was interfaced with a constant current stimulator to administer the electrical stimuli (see *Stimulus* section). Data acquisition occurred directly on the myRIO-1900 at a sampling rate of 200 Hz. Both the microcontroller and stimulator were powered by a 12-V battery (TalentCell, China), and the participants wore all components within a compact backpack. A wireless connection facilitated communication between a laptop (ThinkPad X1 Nano, Lenovo) and the myRIO-1900, enabling system control and real-time data visualization. The myRIO-1900 has a storage capacity of 256 megabytes, so the data were transferred to the laptop halfway through the data collection to avoid data corruption due to insufficient memory storage.

Stimulus

We applied binaural bipolar electrical vestibular stimulation to the participants via carbon rubber electrodes (9 cm^2) coated with conductive gel. The electrodes were affixed to the participant's mastoid processes with hypoallergenic tape. The electrical vestibular stimuli were generated as stochastic waveforms (stochastic EVS; 0–20 Hz, amplitude peak ± 4.5 mA, root mean square 1.25 mA) using LabVIEW 2019b (National Instruments) and were delivered by a constant current isolated linear stimulator (STIMSOLA, Biopac Systems Inc.). We selected these parameters because they have previously been shown to elicit EVS-evoked balance responses in the lower limbs and whole body, with kinematic responses occurring at frequencies between 0–10 Hz during locomotion[22]. Ten unique EVS waveforms were generated for this study, and one was randomly selected for each trial.

EVS modulates the firing rate of the primary otolith and semicircular canal vestibular afferents[52,59,60] to generate craniocentric virtual head movement signals[61,62]. In a binaural bipolar configuration, the EVS-evoked net motion includes a virtual angular velocity signal, oriented around an axis positioned approximately 17–19 degrees above Reid's plane[23,53,63] accompanied by an inference of interaural linear acceleration during a head forward orientation[64]. The choice of stochastic EVS as the stimulus was based on its advantageous characteristics, as it enables the examination of vestibular responses throughout the entire stride cycle[27]. Importantly, stochastic EVS minimizes testing duration when compared to conventional square wave stimuli[27].

Protocol

The protocol for this study was completed outdoors on pavement at the University of British Columbia Vancouver campus. We chose this outdoor setting because there are differences in head kinematics between treadmill and above ground locomotion[9,65,66], so it was important to study head kinematic variability in real-world environments to characterize natural locomotor behaviour. To minimize any possible effects of different locations or ground types, all trials were completed within the same 500-m stretch of walking path. All trials were completed without any precipitation present.

Firstly, to determine their natural walking speed and cadence, participants walked without stimulation for 30 s continuously. The participants were all told to "walk at a normal, comfortable speed" to avoid any possible variation due to different instructions[29]. Additionally, for all trials, we instructed participants to look towards the horizon while walking. While participants are generally instructed to pitch their head at ~ 17–19° from horizontal during studies involving EVS[23], here we were interested in observing natural head kinematics so we chose not to rigidly constrain head pitch during the experiment (see Discussion).

Once the participant's natural locomotor cadence was determined, they completed the following six locomotor cadence conditions in a randomized order: 40%, 60%, 80%, 100%, 120%, and 140% of their natural cadence. The cadences were guided by a metronome played to the participants using earbud headphones and verbal feedback from the experimenter was provided if the participant was not maintaining the desired cadence. We calculated the distance covered from the start to the end of each trial by utilizing global positioning system measurements from a smartphone app (phyphox, RWTH Aachen University). This allowed us to estimate the average gait speed (distance travelled divided by trial duration). For each condition, participants completed 85 strides without any stimulation followed by 215 strides with EVS which was split over three trials. As trial duration was determined by the number of strides and step cadence, it ranged from 65 to 325 s. Trials began when the participant reached the required cadence. While 250 strides has previously been shown to be an appropriate number of strides to characterize time-dependent coherence for lower limb muscles[27], our recent work suggests that fewer strides (up to 120 strides) are needed to estimate vestibular-evoked responses with body mounted IMUs for slow cadences (52 and 78 steps/min) and speeds (~ 0.4 and ~ 0.8 m/s)[22]. Breaks were provided whenever necessary to avoid fatigue and a forced break was taken at the halfway point of the experiment. Prior to and after each trial, the experimenters confirmed that the EVS electrodes and IMUs were secured.

Signal analysis

After data collection, the signals were linearly interpolated to correct for any possible missed samples during data recording. On average, 2.4 samples recorded by the portable system were dropped each trial (range = 0–46 samples), which is approximately one sample dropped for every 22,900 samples, or 115 s. Following the IMU calibration, we filtered the IMU data with a dual pass lowpass fourth order Butterworth filter at 80 Hz. The stochastic EVS data were filtered at 20 Hz with a dual pass lowpass fourth order Butterworth filter.

IMU orientation estimation

To determine the orientation of the various body segments, we used a complementary filter[67] to calculate the tilt orientation of the IMUs along the pitch (around Y-axis) and roll (around X-axis) axes (Eq. 1).

$$\boldsymbol{\theta_i} = \left(\boldsymbol{\theta_{i-1}} + \boldsymbol{\omega_{i,r}} * \boldsymbol{dt}\right)\boldsymbol{G} + \left(\boldsymbol{acc_i}\right)\left(1 - \boldsymbol{G}\right) \tag{1}$$

Here, $\boldsymbol{\theta_i}$ represents the orientation estimate (pitch or roll) at the ith sample point with respect to the vertical axis in one dimension. $\boldsymbol{\omega_{i,r}}$ is the rotated angular velocity around the same axis obtained from the gyroscope (see Eq. 4), $\boldsymbol{dt}$ is the time step between samples (5 ms), $\boldsymbol{G}$ is a weighting factor balancing gyroscope and accelerometer estimates (set to 0.995), and $\boldsymbol{acc_i}$ represents the orientation estimate derived from accelerometer data. If the net acceleration deviated by 10% or more from 9.81 m/s^2, only gyroscope information was used for orientation estimation at that specific sample point.

The equations for calculating accelerometer orientation estimates in pitch and roll, with reference to the IMU body frame and the recorded accelerations ($\boldsymbol{a} = \begin{bmatrix} \ddot{\boldsymbol{x}} & \ddot{\boldsymbol{y}} & \ddot{\boldsymbol{z}} \end{bmatrix}$) were as follows (Eqs. 2 and 3):

$$\boldsymbol{pitch} = \boldsymbol{acc_i} = \boldsymbol{atan2d}(\ddot{\boldsymbol{x}}_i, \ddot{\boldsymbol{z}}_i) \tag{2}$$

$$\boldsymbol{roll} = \boldsymbol{acc_i} = -\boldsymbol{atan2d}\left(\ddot{\boldsymbol{y}}_i, \sqrt{\ddot{\boldsymbol{x}}_i^2 + \ddot{\boldsymbol{z}}_i^2}\right) \tag{3}$$

Additionally, we rotated the raw angular velocities ($\boldsymbol{\omega_i}$) with the previous estimated rotation matrix ($\boldsymbol{R_{i-1}}$, calculated from pitch and roll orientations, assuming no yaw) prior to the complementary filter integration (Eq. 4). This was done to account for the rotating frame during the integration of angular velocity to position.

$$\boldsymbol{\omega_{i,r}} = \boldsymbol{\omega_i}\boldsymbol{R_{i-1}} \tag{4}$$

IMU linear acceleration gravity correction

Linear accelerometers cannot distinguish between gravitational and inertial accelerations. To isolate the true inertial component of linear accelerations at each timestep ($\boldsymbol{a_i^*}$), we removed the gravitational component (Eq. 5). Using the estimated orientation rotation matrix from the current iteration ($\boldsymbol{R_i}$), we rotated and subtracted the gravitational components ($\boldsymbol{g} = \begin{bmatrix} 0 & 0 & -9.81 \end{bmatrix}$) from the current timestep accelerometer data ($\boldsymbol{a_i}$). Subsequently, we low pass filtered the IMU data at 20 Hz using a dual pass 4th order Butterworth filter.

$$\boldsymbol{a_i^*} = \left(\boldsymbol{a_i} - \boldsymbol{g}\boldsymbol{R_i}\right) \tag{5}$$

Head IMU linear acceleration transformation

Finally, to accurately represent linear accelerations experienced by the vestibular system, the linear accelerations were transformed to the location of the vestibular system (approximated as the mid-point between the external acoustic meati) with the following rigid body vector relationship[54,68] (Eq. 6):

$$\boldsymbol{a}_{B,i} = \boldsymbol{a}_{\boldsymbol{A},i} + \boldsymbol{\alpha}_{\boldsymbol{i}} \times \boldsymbol{r}_{\boldsymbol{B-A}} + \boldsymbol{\omega}_{\boldsymbol{i}} \times (\boldsymbol{\omega}_{\boldsymbol{i}} \times \boldsymbol{r}_{\boldsymbol{B-A}}) \tag{6}$$

where $\boldsymbol{a}_{B,i}$ represents the gravity-removed linear acceleration at the approximate location of the vestibular system, $\boldsymbol{a}_{\boldsymbol{A},i}$ is the gravity-removed linear acceleration at the mouthguard, $\boldsymbol{\alpha}_{\boldsymbol{i}}$ denotes angular acceleration, $\boldsymbol{r}_{\boldsymbol{B-A}}$ signifies the position vector from the mouthguard to the approximate location of the vestibular system, and $\boldsymbol{\omega}_{\boldsymbol{i}}$ represents the body-fixed angular velocity.

Step detection

We segmented the data into strides by identifying heel strike and toe-off events using both the right and left ankle IMUs. We determined heel strikes as the local minima of the y-axis angular velocity (mediolateral) following the prominent mid-swing peaks, while we estimated toe-offs as the zero-crossing points of y-axis angular velocity before the mid-swing peaks[55]. We defined a stride as the interval between right heel contact and the sample just before the subsequent right heel contact. Strides were not included if they contained a stumble or trip. We also had a provision to remove strides if they were either 50% longer or shorter than the participant's average stride duration. This resulted in the removal of two total strides across all participants and conditions (both in the same participant at the slowest cadence condition during the EVS trials).

Quantification of head kinematic variability

To assess the variability in head movement during locomotion, we calculated the proportion of residual variance (V_{res}) for both head linear accelerations and angular velocities. This measure was developed to predict the magnitude of vestibular-evoked balance responses during locomotion[16,21]. MacNeilage and Glasauer[16] proposed that the ratio between the residual and total variability of the head kinematics across strides represents the ratio between motor efference copy noise and vestibular information noise, respectively. Based on the Maximum-likelihood model of cue-integration[69,70], they predicted that as vestibular noise increases relative to motor noise, vestibular head motion signals would be downregulated and the vestibular-evoked balance responses would decrease in magnitude. We computed V_{res} for the net head linear acceleration (a_{NET}) and net head angular velocity (ω_{NET}) from the stride-normalized, gravity-corrected, and transformed data from the head IMU. Additionally, we calculated the V_{res} for ML head linear acceleration (a_{ML}) and roll head angular velocity (ω_{roll}) because EVS elicits virtual signals in the frontal plane when walking and looking forward[71,72].

$$\boldsymbol{V}(\boldsymbol{t})_{\boldsymbol{res}} = \boldsymbol{SS}(\boldsymbol{t})_{\boldsymbol{res}} / \boldsymbol{SS}(\boldsymbol{t})_{\boldsymbol{tot}} \tag{7}$$

$$\boldsymbol{SS}(\boldsymbol{t})_{\boldsymbol{res}} = \frac{1}{\boldsymbol{N}} \sum_{\boldsymbol{i}=1}^{\boldsymbol{N}} \sum_{\boldsymbol{d}} \left(\boldsymbol{m}\,(\boldsymbol{t})_{\boldsymbol{d},\boldsymbol{i}} - \boldsymbol{f}\,(\boldsymbol{t})_{\boldsymbol{d}}\right)^2 \tag{8}$$

$$\boldsymbol{SS}(\boldsymbol{t})_{\boldsymbol{tot}} = \frac{1}{\boldsymbol{N}} \sum_{\boldsymbol{i}=1}^{\boldsymbol{N}} \sum_{\boldsymbol{d}} \left(\boldsymbol{m}\,(\boldsymbol{t})_{\boldsymbol{d},\boldsymbol{i}} - \overline{\boldsymbol{m}}_{\boldsymbol{d}}\right)^2 \tag{9}$$

where $\boldsymbol{V}(\boldsymbol{t})_{\boldsymbol{res}}$ is the V_{res} across the stride cycle (Eq. 7), $\boldsymbol{SS}(\boldsymbol{t})_{\boldsymbol{res}}$ is the residual sum of squares representing the deviation from the average stride cycle (i.e., stride-cycle attractor; Eq. 8) and $\boldsymbol{SS}(\boldsymbol{t})_{\boldsymbol{tot}}$ is the total signal magnitude from the total stride cycle mean (Eq. 9). We calculated these measures across the normalized stride cycle between the total number of strides ($\boldsymbol{N}$). $\boldsymbol{d}$ represents the dimension (axes x, y, z) of the head motion. For the V_{res} a_{NET} and V_{res} ω_{NET}, $d = [xyz]$ and the components ($\boldsymbol{SS}(\boldsymbol{t})_{\boldsymbol{res}}$ and $\boldsymbol{SS}(\boldsymbol{t})_{\boldsymbol{tot}}$) were calculated by summing the squared error across all three dimensions. Whereas for the V_{res} a_{ML}, $d = y$ and for the V_{res} ω_{roll}, $d = x$. $\boldsymbol{m}\,(\boldsymbol{t})_{\boldsymbol{d},\boldsymbol{i}}$ is the head motion at the normalized stride time t, for stride i and in dimension d. $\boldsymbol{f}\,(\boldsymbol{t})_{\boldsymbol{d}}$ is the average head motion (stride-cycle attractor) at time t and dimension d. $\overline{\boldsymbol{m}}_{\boldsymbol{d}}$ is the average head motion along the dimension d.

We calculated V_{res} for both the trials with and without the applied EVS. While the average V_{res} was ~ 11–23% higher in the trials with the applied EVS, the changes in V_{res} across step cadences were similar between conditions. Thus, only the V_{res} measures from trials with EVS are shown in the results. The EVS-induced increase in average V_{res} was mainly driven by larger (~ 10–48%) residual variability around the average stride cycle kinematics. The V_{res} measures from the trials without EVS are included in the Supplementary Materials.

Time-dependent frequency analyses

To assess the phasic modulation of vestibular-evoked balance responses during locomotion, we computed time-dependent coherence, gain, and spectral output power between the EVS and body kinematics (gravity-corrected ML acceleration from the low back and ankle IMUs, each calculated individually). Coherence was not calculated using the head kinematics, because these will be affected by both whole-body movements as well as head specific vestibular reflexes (i.e., vestibulocolic reflex) which can occur at frequencies much higher than the applied EVS (up to 300 Hz)[73]. Coherence is a metric for assessing the linear association between an input and output signal across various frequencies. It can be likened to time-domain correlation analyses, wherein a coherence value of 0 indicates no similarity, while a value of 1 indicates a perfect correlation with no noise, irrespective of scaling, between two signals at a specific frequency[28,74]. The coherence between the EVS and low back ML acceleration represents the vestibular response evoked at the body centre of mass, whereas the coherences between the EVS and the ankle ML accelerations represent the vestibular responses evoked in the lower limbs. Gain quantifies the scaling factor between the two signals at a particular frequency while spectral output power characterizes the squared magnitude of the output signal (gravity-corrected ML acceleration from the low back and ankle IMUs) across different frequencies.

We employed Morlet wavelet decomposition spanning from 0.5 Hz to 20 Hz, to extract time-dependent cross-spectra and auto-spectra of EVS and body segment kinematics[27,28,75]. Wavelets were defined in 0.5 Hz intervals, but still have power outside of their peak frequency due to frequency smoothing that occurs when defining the wavelets[76]. The data were divided into strides and padded with 50% additional data from preceding and subsequent strides to prevent distortions at the edge of a window. To maximize coherence between applied EVS and evoked balance responses, we shifted the EVS signal 200 ms later in time[62,77,78] prior to the frequency analyses.

Following the Morlet decomposition, we resampled the data from each stride to facilitate stride-by-stride coherence, gain, and spectral power output calculations. For individual participant results, we normalized stride durations and gait event timings (right heel strike, left toe-off, left heel strike, right toe-off) to each participant's individual averages for the given cadence condition. For between cadence comparisons, normalization was carried out with respect to total means across participants and cadences. This allowed for comparisons throughout the stride cycle while maintaining alignment with gait events. The time-dependent coherence $[\boldsymbol{C}(\boldsymbol{\tau},\boldsymbol{f})]$, gain $[\boldsymbol{G}(\boldsymbol{\tau},\boldsymbol{f})]$, and body kinematics spectral output power $[\boldsymbol{S}(\boldsymbol{\tau},\boldsymbol{f})]$ were calculated using the following Eqs. (10–12):

$$\boldsymbol{C}(\boldsymbol{\tau},\boldsymbol{f})=\frac{|\boldsymbol{P_{xy}}(\boldsymbol{\tau},\boldsymbol{f})|^2}{\boldsymbol{P_{xx}}(\boldsymbol{\tau},\boldsymbol{f})\,\boldsymbol{P_{yy}}(\boldsymbol{\tau},\boldsymbol{f})} \tag{10}$$

$$\boldsymbol{G}(\boldsymbol{\tau},\boldsymbol{f})=\left|\frac{\boldsymbol{P_{xy}}(\boldsymbol{\tau},\boldsymbol{f})}{\boldsymbol{P_{xx}}(\boldsymbol{\tau},\boldsymbol{f})}\right| \tag{11}$$

$$\boldsymbol{S}(\boldsymbol{\tau},\boldsymbol{f})=\boldsymbol{P_{yy}}(\boldsymbol{\tau},\boldsymbol{f}) \tag{12}$$

where $\boldsymbol{\tau}$ represents the specific time point within the stride cycle, and $\boldsymbol{f}$ is the frequency. $\boldsymbol{P_{xy}}(\boldsymbol{\tau},\boldsymbol{f})$ represents the time-normalized time-dependent cross-spectrum between EVS and body kinematics (low back or ankle ML linear acceleration), $\boldsymbol{P_{xx}}(\boldsymbol{\tau},\boldsymbol{f})$ is the time-normalized time-dependent auto-spectrum of the EVS signal, and $\boldsymbol{P_{yy}}(\boldsymbol{\tau},\boldsymbol{f})$ is the time-normalized time-dependent auto-spectrum of body kinematic measurements (low back or ankle ML linear acceleration) obtained from the IMU.

Data reduction & statistical analysis

We reported summary statistics as mean ± SD. To address the main objectives of this study, we performed the following analyses to examine the changes in the V_{res} and vestibular-evoked balance responses across cadences spanning 40–140% of each participant's preferred cadence.

Determining coherence significance

For each participant, we determined time-dependent coherence to be significant if it crossed a 99% confidence limit ($\boldsymbol{CL}=0.01$) threshold which is equivalent to an alpha-level of 0.05 due to the two-dimensional (time and frequency) nature of the data[27]. Based on the number of strides ($\boldsymbol{n}=215$) used to calculate coherence, we determined the threshold for each participant was 0.0212 (99%; Eq. 13).

$$\boldsymbol{threshold}=1-\boldsymbol{CL}^{1/\boldsymbol{n}} \tag{13}$$

We performed similar calculations for the pooled time-dependent coherence; however, pooled time-dependent coherence was calculated by using the sum of all the cross- and auto-spectra, consequently the significance threshold was determined by the total number of strides summed across the participants ($\boldsymbol{n}=2580$). This resulted in a significance threshold for the pooled time-dependent coherence of 0.0018 (99%).

Comparison of head kinematic variability and vestibular control across cadences

To compare changes to head kinematic variability, we extracted mean V_{res} across the stride cycle (for all four measures calculated) from each participant and cadence. This approach has previously been used to compare the attenuation of vestibular-evoked balance responses and V_{res} between different cadences and speeds[21,22]. Similarly, we extracted peak coherence (across time and frequency) from each participant and cadence for the back, right ankle and left ankle ML acceleration to quantify vestibular-evoked balance responses across the cadences. To correct for the non-normality of these values, we applied a Fisher transformation[79]. While coherence and gain have been used in tandem to quantify vestibular-evoked balance responses[27], gain is unreliable at low and non-significant coherences. Given that we observed low (or non-significant) coherence at the higher step cadence conditions, we only used coherence to quantify the vestibular-evoked balance responses but present power and gain estimates in Fig. 5 (see Results) as well as bootstrapped differences in the Supplementary Materials.

To determine the main effects of step cadence on V_{res} and coherence, we performed independent rmANOVAs ($\alpha=0.05$) for all four V_{res} measures and all three coherence measures[80]. When the assumption of sphericity was violated, a Greenhouse–Geisser correction was performed. We then performed post-hoc paired Student t-tests to compare between specific step cadence conditions. To confirm previous observations, that both V_{res} and coherence decrease from slow step cadences (below preferred step cadence) up to preferred step cadences[21,22], one-sided Student t-tests were performed between the 40% and 100% step cadence condition. Similarly, to confirm that coherence continued to decrease at step cadences faster than preferred cadence, we performed one-sided Student t-tests between the 100% and 120% as well as 100% and 140% step cadence conditions. Given that it was not clear how V_{res} would change at faster step cadences, we performed two-sided Student t-tests to compare the 100% to the 120% and to the 140% conditions. The Holm method was used to correct for the multiple comparisons[81].

To directly compare the relationship between V_{res} and coherence, we calculated the coefficient of determination (R^2) of a linear fit between each combination of mean V_{res} and peak coherence measures. This was calculated for the 40% to 100% step cadence conditions, the 100% to 140% step cadence conditions, and all step cadence conditions. Thus, we compared the linear fits and the R^2 values between fits to determine how the relationship between V_{res} and coherence changed across step cadences.

Curve fitting mean V_{res} and peak coherence across cadences and speeds

To model the changes in mean V_{res} and peak coherence across cadences, we performed curve fitting to both the group and individual participant responses to characterize how these measures changed as a function of step cadence. Even though participants walked at a wide range of cadences, we did not normalize the cadences relative to the preferred cadence to facilitate comparisons with existing literature on average preferred step cadences[30–32]. As the V_{res} measures were variable between participants, we normalized each participant's average mean V_{res} to the overall average mean V_{res} across participants for each measure. Given that we expected coherence to decrease as step cadence increases, we fitted an exponential decay function to the extracted peak coherences for each participant and the three coherence measures calculated. We also fitted an exponential decay to the mean V_{res} measures across cadences to test if V_{res} would similarly decrease (Eq. 14), given that MacNeilage & Glasauer (2017) proposed it as a measure to predict changes to vestibular balance responses.

$$\boldsymbol{y} = \boldsymbol{a}e^{\boldsymbol{bx}} \tag{14}$$

where $\boldsymbol{a}$ and $\boldsymbol{b}$ were evaluated using a non-linear least squares fitting method, $\boldsymbol{b} < 0$ in order to model a decay function, $\boldsymbol{x}$ is the cadence, and $\boldsymbol{y}$ is the predicted measure (peak coherence or mean V_{res}). We then calculated the adjusted coefficient of determination ($\overline{R}^2$) for each of the individual participant fits.

In order to determine whether V_{res} was minimal near preferred cadences and could better be modelled as a polynomial function, we also fit a 2nd degree polynomial to the extracted values (Eq. 15). This was only performed for the V_{res} given that previous work suggest that vestibular-evoked balance responses will decrease with increased step cadence and speed and thus it was not expected to increase above the preferred step cadence[13,15,21,22].

$$\boldsymbol{y} = \boldsymbol{a}\boldsymbol{x}^2 + \boldsymbol{b}\boldsymbol{x} + \boldsymbol{c} \tag{15}$$

where $\boldsymbol{a}$, $\boldsymbol{b}$, and $\boldsymbol{c}$ were fitted with least squares, $\boldsymbol{x}$ is the cadence, and $\boldsymbol{y}$ is the predicted measure (mean V_{res}). To compare the fits for mean V_{res}, we calculated the Akaike information criterion (AIC) for the group exponential decay and polynomial fits[82]. Given that a lower AIC value indicates a better fit, accounting for the number of parameters, we calculated the difference in the AIC (ΔAIC) as the AIC from the polynomial subtracted by the AIC from the exponential decay.

Similar to step cadence, we also performed the same curve fitting for the mean V_{res} and peak coherence across average gait speed, which we calculated using the distance travelled and trial duration. We performed these additional analyses to facilitate comparisons with the existing locomotor energetics literature[4,5], which quantified changes to metabolic cost across gait speeds. While step cadence and gait speed are strongly related[83], the relationship between step cadence and gait speed was not perfectly linear because we did not control step length.

Data availability

Data and code to replicate the figures in this manuscript can be found in the Borealis data repository (https://doi.org/10.5683/SP3/LLLEF8).

Received: 26 August 2024; Accepted: 23 April 2025
Published online: 28 May 2025

References

1. Faisal, A. A., Selen, L. P. & Wolpert, D. M. Noise in the nervous system. *Nat. Rev. Neurosci.* **9**, 292–303 (2008).
2. Angelaki, D. E. & Cullen, K. E. Vestibular system: The many facets of a multimodal sense. *Annu. Rev. Neurosci.* **31**, 125–150 (2008).
3. Day, B. L. & Fitzpatrick, R. C. The vestibular system. *Curr. Biol.* **15**, R583–R586 (2005).
4. Ralston, H. J. Energy-speed relation and optimal speed during level walking. *Int. Z. Angew. Physiol. Einschl. Arbeitsphysiol.* **17**, 277–283 (1958).
5. Zarrugh, M. Y., Todd, F. N. & Ralston, H. J. Optimization of energy expenditure during level walking. *Eur. J. Appl. Physiol.* **33**, 293–306 (1974).
6. Selinger, J. C., O'Connor, S. M., Wong, J. D. & Donelan, J. M. Humans can continuously optimize energetic cost during walking. *Curr. Biol.* **25**, 2452–2456 (2015).
7. Laughlin, S. Energy as a constraint on the coding and processing of sensory information. *Curr. Opin. Neurobiol.* **11**, 475–480 (2001).

8. Cromwell, R. L. et al. Adaptations in horizontal head stabilization in response to altered vision and gaze during natural walking. *J. Vestib. Res.: Equilib. Orientat.* **14**, 367–373 (2004).
9. Hirasaki, E., Moore, S. T., Raphan, T. & Cohen, B. Effects of walking velocity on vertical head and body movements during locomotion. *Exp. Brain Res.* **127**, 117–130 (1999).
10. Mulavara, A. P. & Bloomberg, J. J. Identifying head-trunk and lower limb contributions to gaze stabilization during locomotion. *J. Vestib. Res.* **12**, 255–269 (2002).
11. Pozzo, T., Berthoz, A. & Lefort, L. Head stabilization during various locomotor tasks in humans. *Exp. Brain Res* **82**, 97–106 (1990).
12. Brandt, T., Strupp, M. & Benson, J. You are better off running than walking with acute vestibulopathy. *Lancet* **354**, 746 (1999).
13. Dakin, C. J., Inglis, J. T., Chua, R. & Blouin, J.-S. Muscle-specific modulation of vestibular reflexes with increased locomotor velocity and cadence. *J. Neurophysiol.* **110**, 86–94 (2013).
14. Iles, J. F., Baderin, R., Tanner, R. & Simon, A. Human standing and walking: Comparison of the effects of stimulation of the vestibular system. *Exp. Brain Res.* **178**, 151–166 (2007).
15. Jahn, K., Strupp, C. A. M., Schneider, E., Dieterich, M. & Brandt, T. Differential effects of vestibular stimulation on walking and running. *NeuroReport* **11**, 1745–1748 (2000).
16. MacNeilage, P. R. & Glasauer, S. Quantification of head movement predictability and implications for suppression of vestibular input during locomotion. *Front. Comput. Neurosci.* **11**, 47 (2017).
17. Lambert, F. M., Combes, D., Simmers, J. & Straka, H. Gaze stabilization by efference copy signaling without sensory feedback during vertebrate locomotion. *Curr. Biol.* **22**, 1649–1658 (2012).
18. Lambert, F. M., Beraneck, M., Straka, H. & Simmers, J. Locomotor efference copy signaling and gaze control: An evolutionary perspective. *Curr Opin Neurobiol* **82**, 102761 (2023).
19. von Uckermann, G., Le Ray, D., Combes, D., Straka, H. & Simmers, J. Spinal efference copy signaling and gaze stabilization during locomotion in juvenile Xenopus frogs. *J. Neurosci.* **33**, 4253–4264 (2013).
20. Mackrous, I., Carriot, J. & Cullen, K. E. Context-independent encoding of passive and active self-motion in vestibular afferent fibers during locomotion in primates. *Nat. Commun.* **13**, 120 (2022).
21. Dietrich, H. et al. Head motion predictability explains activity-dependent suppression of vestibular balance control. *Sci. Rep.* **10**, 1–10 (2020).
22. Foulger, L. H., Charlton, J. M. & Blouin, J.-S. Real-world characterization of vestibular contributions during locomotion. *Front. Hum. Neurosci.* **17**, 9097 (2024).
23. Fitzpatrick, R. C. & Day, B. L. Probing the human vestibular system with galvanic stimulation. *J. Appl. Physiol.* **96**, 2301–2316 (2004).
24. Kirtley, C., Whittle, M. W. & Jefferson, R. J. Influence of walking speed on gait parameters. *J. Biomed. Eng.* **7**, 282–288 (1985).
25. Nymark, J. R., Balmer, S. J., Melis, E. H., Lemaire, E. D. & Millar, S. Electromyographic and kinematic nondisabled gait differences at extremely slow overground and treadmill walking speeds. *JRRD* **42**, 523 (2005).
26. Wu, A. R., Simpson, C. S., van Asseldonk, E. H. F., van der Kooij, H. & Ijspeert, A. J. Mechanics of very slow human walking. *Sci. Rep.* **9**, 18079 (2019).
27. Blouin, J.-S. et al. Extracting phase-dependent human vestibular reflexes during locomotion using both time and frequency correlation approaches. *J. Appl. Physiol.* **111**, 1484–1490 (2011).
28. Zhan, Y., Halliday, D., Jiang, P., Liu, X. & Feng, J. Detecting time-dependent coherence between non-stationary electrophysiological signals—A combined statistical and time–frequency approach. *J. Neurosci. Methods* **156**, 322–332 (2006).
29. Brinkerhoff, S. A., Murrah, W. M., Hutchison, Z., Miller, M. & Roper, J. A. Words matter: Instructions dictate "self-selected" walking speed in young adults. *Gait Posture* **95**, 223–226 (2022).
30. Latt, M. D., Menz, H. B., Fung, V. S. & Lord, S. R. Walking speed, cadence and step length are selected to optimize the stability of head and pelvis accelerations. *Exp. Brain Res.* **184**, 201–209 (2007).
31. Menz, H. B., Lord, S. R. & Fitzpatrick, R. C. Acceleration patterns of the head and pelvis when walking on level and irregular surfaces. *Gait Posture* **18**, 35–46 (2003).
32. Renggli, D. et al. Wearable inertial measurement units for assessing gait in real-world environments. *Front. Physiol.* **11**, 90 (2020).
33. Russell, D. M. & Apatoczky, D. T. Walking at the preferred stride frequency minimizes muscle activity. *Gait Posture* **45**, 181–186 (2016).
34. Sekiya, N., Nagasaki, H., Ito, H. & Furuna, T. Optimal walking in terms of variability in step length. *J. Orthop. Sports Phys. Ther.* **26**, 266–272 (1997).
35. Inman, V. T., Ralston, H. J., Todd, F. & Lieberman, J. C. *Human Walking* (Williams & Wilkins, 1981).
36. Waters, R. L., Lunsford, B. R., Perry, J. & Byrd, R. Energy-speed relationship of walking: Standard tables. *J. Orthop. Res.* **6**, 215–222 (1988).
37. Bellanca, J. L., Lowry, K. A., VanSwearingen, J. M., Brach, J. S. & Redfern, M. S. Harmonic ratios: A quantification of step to step symmetry. *J. Biomech.* **46**, 828–831 (2013).
38. Pasciuto, I., Bergamini, E., Iosa, M., Vannozzi, G. & Cappozzo, A. Overcoming the limitations of the harmonic ratio for the reliable assessment of gait symmetry. *J. Biomech.* **53**, 84–89 (2017).
39. Fechner, G. T., Adler, H. E., Howes, D. H. & Boring, E. G. *Elements of Psychophysics* (Holt, Rinehart and Winston, 1966).
40. Mallery, R. M., Olomu, O. U., Uchanski, R. M., Militchin, V. A. & Hullar, T. E. Human discrimination of rotational velocities. *Exp. Brain Res.* **204**, 11–20 (2010).
41. Carriot, J., Cullen, K. E. & Chacron, M. J. The neural basis for violations of Weber's law in self-motion perception. *Proc. Natl. Acad. Sci. U.S.A.* **118**, e2025061118 (2021).
42. Harris, J. J., Jolivet, R., Engl, E. & Attwell, D. Energy-efficient information transfer by visual pathway synapses. *Curr. Biol.* **25**, 3151–3160 (2015).
43. Niven, J. E. Neuronal energy consumption: Biophysics, efficiency and evolution. *Curr. Opin. Neurobiol.* **41**, 129–135 (2016).
44. Niven, J. E. & Laughlin, S. B. Energy limitation as a selective pressure on the evolution of sensory systems. *J. Exp. Biol.* **211**, 1792–1804 (2008).
45. Antos, S. A., Kording, K. P. & Gordon, K. E. Energy expenditure does not solely explain step length–width choices during walking. *J. Exp. Biol.* **225**, jeb243104 (2022).
46. Wong, J. D., O'Connor, S. M., Selinger, J. C. & Donelan, J. M. Contribution of blood oxygen and carbon dioxide sensing to the energetic optimization of human walking. *J. Neurophysiol.* **118**, 1425–1433 (2017).
47. Cullen, K. E. Vestibular processing during natural self-motion: Implications for perception and action. *Nat. Rev. Neurosci.* **20**, 346–363 (2019).
48. Magnani, R. M., Bruijn, S. M., van Dieën, J. H. & Forbes, P. A. Stabilization demands of walking modulate the vestibular contributions to gait. *Sci. Rep.* **11**, 13736 (2021).
49. Forbes, P. A. et al. Rapid limb-specific modulation of vestibular contributions to ankle muscle activity during locomotion. *J. Physiol.* **595**, 2175–2195 (2017).
50. Schneider, A. D., Jamali, M., Carriot, J., Chacron, M. J. & Cullen, K. E. The increased sensitivity of irregular peripheral canal and otolith vestibular afferents optimizes their encoding of natural stimuli. *J. Neurosci.* **35**, 5522–5536 (2015).
51. Massot, C., Schneider, A. D., Chacron, M. J. & Cullen, K. E. The vestibular system implements a linear-nonlinear transformation in order to encode self-motion. *PLoS Biol.* **10**, e1001365 (2012).

52. Kwan, A., Forbes, P. A., Mitchell, D. E., Blouin, J.-S. & Cullen, K. E. Neural substrates, dynamics and thresholds of galvanic vestibular stimulation in the behaving primate. *Nat. Commun.* **10**, 1 (2019).
53. Chen, A., Khosravi-Hashemi, N., Kuo, C., Kramer, J. K. & Blouin, J. S. Development of a conversion model between mechanical and electrical vestibular stimuli. *J. Neurophysiol.* **123**, 548–559 (2020).
54. Wu, L. C. et al. In vivo evaluation of wearable head impact sensors. *Ann. Biomed. Eng.* **44**, 1234–1245 (2016).
55. Bötzel, K., Marti, F. M., Rodríguez, M. Á. C., Plate, A. & Vicente, A. O. Gait recording with inertial sensors – How to determine initial and terminal contact. *J. Biomech.* **49**, 332–337 (2016).
56. de Melker Worms, J. L. A., Stins, J. F., Beek, P. J. & Loram, I. D. The effect of fear of falling on vestibular feedback control of balance. *Physiol. Rep.* **5**, e13391 (2017).
57. Geist, J., Afridi, M. Y., McGray, C. D. & Gaitan, M. Gravity-based characterization of three-axis accelerometers in terms of intrinsic accelerometer parameters. *J. Res. Natl. Inst. Stan.* **122**, 32 (2017).
58. Chen, A., Kuo, C. & Blouin, J.-S. A portable and low-cost solution for real-time manipulation of the vestibular sense. *J. Neurosci. Methods* **382**, 109709 (2022).
59. Goldberg, J. M., Fernandez, C. & Smith, C. E. Responses of vestibular-nerve afferents in the squirrel monkey to externally applied galvanic currents. *Brain Res.* **252**, 156–160 (1982).
60. Forbes, P. A., Kwan, A., Mitchell, D. E., Blouin, J.-S. & Cullen, K. E. The neural basis for biased behavioral responses evoked by galvanic vestibular stimulation in primates. *J. Neurosci.* **43**, 1905–1919 (2023).
61. Lund, S. & Broberg, C. Effects of different head positions on postural sway in man induced by a reproducible vestibular error signal. *Acta Physiol. Scand.* **117**, 307 (1983).
62. Mian, O. S. & Day, B. L. Violation of the craniocentricity principle for vestibularly evoked balance responses under conditions of anisotropic stability. *J. Neurosci.* **34**, 7696–7703 (2014).
63. Schneider, E., Glasauer, S. & Dieterich, M. Comparison of human ocular torsion patterns during natural and galvanic vestibular stimulation. *J. Neurophysiol.* **87**, 2064–2073 (2002).
64. Khosravi-Hashemi, N., Forbes, P. A., Dakin, C. J. & Blouin, J. Virtual signals of head rotation induce gravity-dependent inferences of linear acceleration. *J. Physiol.* **597**, 5231–5246 (2019).
65. Bloomberg, J. J., Reschke, M. F., Huebner, W. P. & Peters, B. T. The effects of target distance on eye and head movement during locomotion. *Ann. N. Y. Acad. Sci.* **656**, 699–707 (1992).
66. Hirasaki, E., Kubo, T., Nozawa, S., Matano, S. & Matsunaga, T. Analysis of head and body movements of elderly people during locomotion. *Acta Otolaryngol.* **113**, 25–30 (1993).
67. Gui, P., Tang, L. & Mukhopadhyay, S. MEMS based IMU for tilting measurement: Comparison of complementary and Kalman filter based data fusion. In *2015 IEEE 10th Conference on Industrial Electronics and Applications (ICIEA)* 2004–2009 (2015). https://doi.org/10.1109/ICIEA.2015.7334442.
68. Blouin, J.-S., Siegmund, G. P. & Timothy Inglis, J. Interaction between acoustic startle and habituated neck postural responses in seated subjects. *J. Appl. Physiol.* **102**, 1574–1586 (2007).
69. van Beers, R. J., Sittig, A. C. & Denier Van Der Gon, J. J. Integration of proprioceptive and visual position-information: An experimentally supported model. *J. Neurophysiol.* **81**, 1355–1364 (1999).
70. Ernst, M. O. & Banks, M. S. Humans integrate visual and haptic information in a statistically optimal fashion. *Nature* **415**, 429–433 (2002).
71. Bent, L. R., Inglis, J. T. & McFadyen, B. J. When is vestibular information important during walking?. *J. Neurophysiol.* **92**, 1269–1275 (2004).
72. Fitzpatrick, R. C., Butler, J. E. & Day, B. L. Resolving head rotation for human bipedalism. *Curr. Biol.* **16**, 1509–1514 (2006).
73. Forbes, P. A. et al. Neural mechanisms underlying high-frequency vestibulocollic reflexes in humans and monkeys. *J. Neurosci.* **40**, 1874–1887 (2020).
74. van Drongelen, W. *Signal Processing for Neuroscientists: Introduction to the Analysis of Physiological Signals* (Elsevier/Academic Press, 2007).
75. Cohen, M. X. A better way to define and describe Morlet wavelets for time-frequency analysis. *Neuroimage* **199**, 81–86 (2019).
76. Cohen, M. X. *Analyzing Neural Time Series Data: Theory and Practice* (The MIT Press, 2014).
77. Dalton, B. H., Blouin, J.-S., Allen, M. D., Rice, C. L. & Inglis, J. T. The altered vestibular-evoked myogenic and whole-body postural responses in old men during standing. *Exp. Gerontol.* **60**, 120–128 (2014).
78. Tisserand, R. et al. Down regulation of vestibular balance stabilizing mechanisms to enable transition between motor states. *Elife* **7**, e36123 (2018).
79. Grosse, P. & Brown, P. Acoustic startle evokes bilaterally synchronous oscillatory EMG activity in the healthy human. *J. Neurophysiol.* **90**, 1654–1661 (2003).
80. JASP Team. JASP (Version 0.17.3) [Computer software] (2023).
81. Holm, S. A simple sequentially rejective multiple test procedure. *Scand. J. Stat.* **6**, 65–70 (1979).
82. Akaike, H. A new look at the statistical model identification. *IEEE Trans. Autom. Control* **19**, 716–723 (1974).
83. Uchida, T. K. & Delp, S. L. *Biomechanics of Movement: The Science of Sports, Robotics, and Rehabilitation* (MIT Press, 2021).

Acknowledgements

We would like to thank Aidan Della Siega and Matthew Galassi for their help with data collection as well as Drs. Chris Dakin and Patrick Forbes for their comments on the manuscript.

Author contributions

LHF—Conceptualization, Methodology, Formal analysis, Investigation, Writing—Original Draft, Writing—Review & Editing; CK—Methodology, Writing—Review & Editing; RC—Writing—Review & Editing; JSB—Conceptualization, Methodology, Resources, Writing—Review & Editing, Supervision, Funding acquisition.

Declarations

Competing interests

The authors declare no competing interests.

Additional information

Supplementary Information The online version contains supplementary material available at https://doi.org/10.1038/s41598-025-99878-w.

Correspondence and requests for materials should be addressed to J.-S.B.

Reprints and permissions information is available at www.nature.com/reprints.

Publisher's Note Springer Nature remains neutral with regard to jurisdictional claims in published maps and institutional affiliations.

Open Access This article is licensed under a Creative Commons Attribution-NonCommercial-NoDerivatives 4.0 International License, which permits any non-commercial use, sharing, distribution and reproduction in any medium or format, as long as you give appropriate credit to the original author(s) and the source, provide a link to the Creative Commons licence, and indicate if you modified the licensed material. You do not have permission under this licence to share adapted material derived from this article or parts of it. The images or other third party material in this article are included in the article's Creative Commons licence, unless indicated otherwise in a credit line to the material. If material is not included in the article's Creative Commons licence and your intended use is not permitted by statutory regulation or exceeds the permitted use, you will need to obtain permission directly from the copyright holder. To view a copy of this licence, visit http://creativecommons.org/licenses/by-nc-nd/4.0/.

© The Author(s) 2025